Volume 188
Number 15
July 24, 2025

Cell

CellPress

Cell

Article

Fragmented replay of very large environments in the hippocampus of bats

Graphical abstract

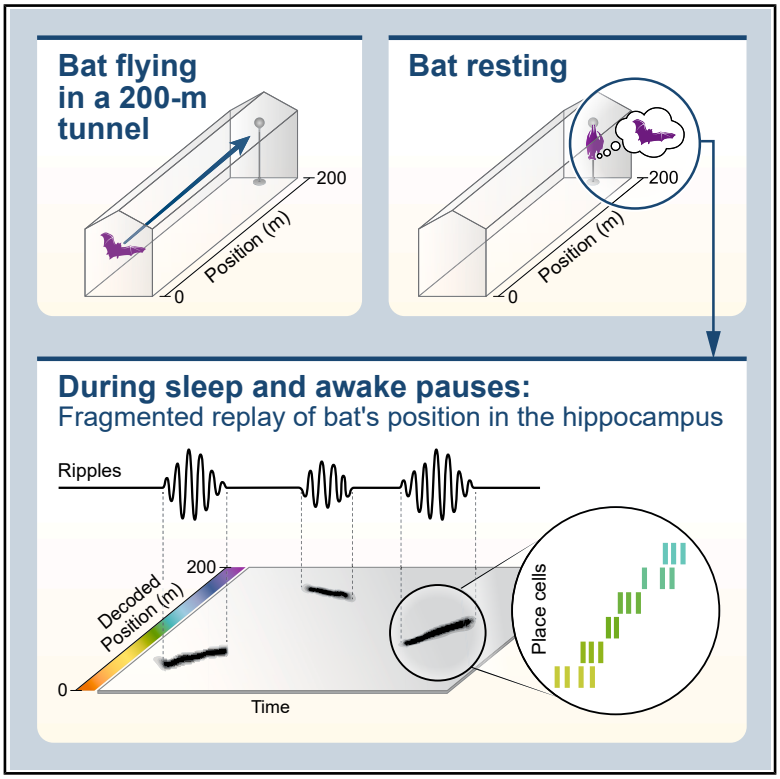

Authors

Tamir Eliav, Shir R. Maimon, Ayelet Sarel, Shaked Palgi, Liora Las, Nachum Ulanovsky

Correspondence

nachum.ulanovsky@weizmann.ac.il

In brief

Hippocampal replays in bats flying in a 200-m tunnel depict short fragments of long flight trajectories, suggesting constraints on the mechanisms and functions of replay.

Highlights

- Hippocampal recordings in a large environment reveal naturalistic aspects of replay
- Replays are fragmented, each covering ~6% of the environment
- Replays depict behaviorally relevant events, e.g., landings and conspecific interactions
- Fragmented replays may reflect memory chunking for hippocampal-cortical communication

Eliav et al., 2025, Cell *188*, 4091–4105
July 24, 2025
https://doi.org/10.1016/j.cell.2025.05.024

CellPress

Cell

CellPress

Article

Fragmented replay of very large environments in the hippocampus of bats

Tamir Eliav,[1,2,3] Shir R. Maimon,[1,2] Ayelet Sarel,[1] Shaked Palgi,[1] Liora Las,[1] and Nachum Ulanovsky[1,4,*]
[1]Department of Brain Sciences, Weizmann Institute of Science, Rehovot 76100, Israel
[2]These authors contributed equally
[3]Present address: Max Planck Institute for Biological Intelligence, Seewiesen 82319, Germany
[4]Lead contact
*Correspondence: nachum.ulanovsky@weizmann.ac.il
https://doi.org/10.1016/j.cell.2025.05.024

SUMMARY

The hippocampus is crucial for memory. Memory consolidation is thought to be subserved by hippocampal "replays" of previously experienced trajectories. However, it is unknown how the brain replays long spatial trajectories in very large, naturalistic environments. Here, we investigated this in the hippocampus of bats that were flying prolonged flights in a 200-m-long tunnel. We found many time-compressed replay sequences during sleep and during awake pauses between flights, similar to rodents exploring small environments. Individual neurons fired multiple times per replay, according to their multiple place fields. Surprisingly, replays were highly fragmented, depicting short trajectory pieces covering only ~6% of the environment size—unlike replays in small setups, which cover most of the environment. This fragmented replay may reflect biophysical or network constraints on replay distance and may facilitate memory chunking for hippocampal-neocortical communication. Overall, hippocampal replay in very large environments is radically different from classical notions of memory reactivation—carrying important implications for hippocampal network mechanisms in naturalistic, real-world environments.

INTRODUCTION

The hippocampus plays a key role in various cognitive functions, including spatial navigation and memory.[1–4] Navigation is thought to be subserved by hippocampal place cells—neurons that encode the animal's current location in the environment.[5–9] Memory consolidation, on the other hand, is thought to be subserved by "replay" events in the hippocampus—wherein ensembles of hippocampal place cells exhibit sequential reactivation of previously experienced trajectories.[10–13] Hippocampal replays unfold at a faster speed than the actual behavioral trajectories, thus temporally compressing the original trajectory.[10–17] Such fast neuronal replay sequences are seen during both sleep and awake states and have been studied extensively in rodents navigating in small environments.[14–17] Yet, despite a quarter century of research, the function of hippocampal replay remains debated. One widely held theory suggests that replay is important for memory consolidation. This idea is supported by studies showing that disruption of replay events, and their associated sharp-wave ripples, leads to memory deficits.[18–21] According to this memory-consolidation theory, during "offline" states, such as sleep and awake pauses in behavior, the hippocampus sends "packets" of information to the neocortex—in the form of replays—in order to encode recent events into long-term memory storage.[14,15,22–25] An alternative theory on hippocampal replay suggests that it is not related to *memory* of past events but rather to *planning* of future trajectories.[26,27] However, for both the memory and planning theories of replay, there is a major gap—it is unknown whether and how replays occur in large, naturalistic environments and for prolonged behavioral epochs.

To date, replays were always studied in relatively small environments, typically 1–2 m in size, and up to 10 m[28]—and the replays that were found have typically spanned all or most of the distance traveled within the environment.[10–12,28] It remains unknown how information on very large, natural-scale environments is replayed in the hippocampus. Are there replays on such spatial scales? If so, we posited two possibilities: first, that the entire huge environment would be replayed at an ultra-fast speed. Second, if replay speed is similar in both large and small environments, then the replay duration must be ultra-prolonged in time. Here, we set out to answer these questions by studying bats flying in a very large environment. We observed replays occurring both during sleep and during awake pauses between flights. Surprisingly, however, these replays did not conform to any of the aforementioned two possibilities. Instead, we found an unexpected third option.

RESULTS

Hippocampal replay of a very large 200-m environment

To investigate hippocampal replay in very large environments, we analyzed data from experiments in 7 Egyptian fruit bats,

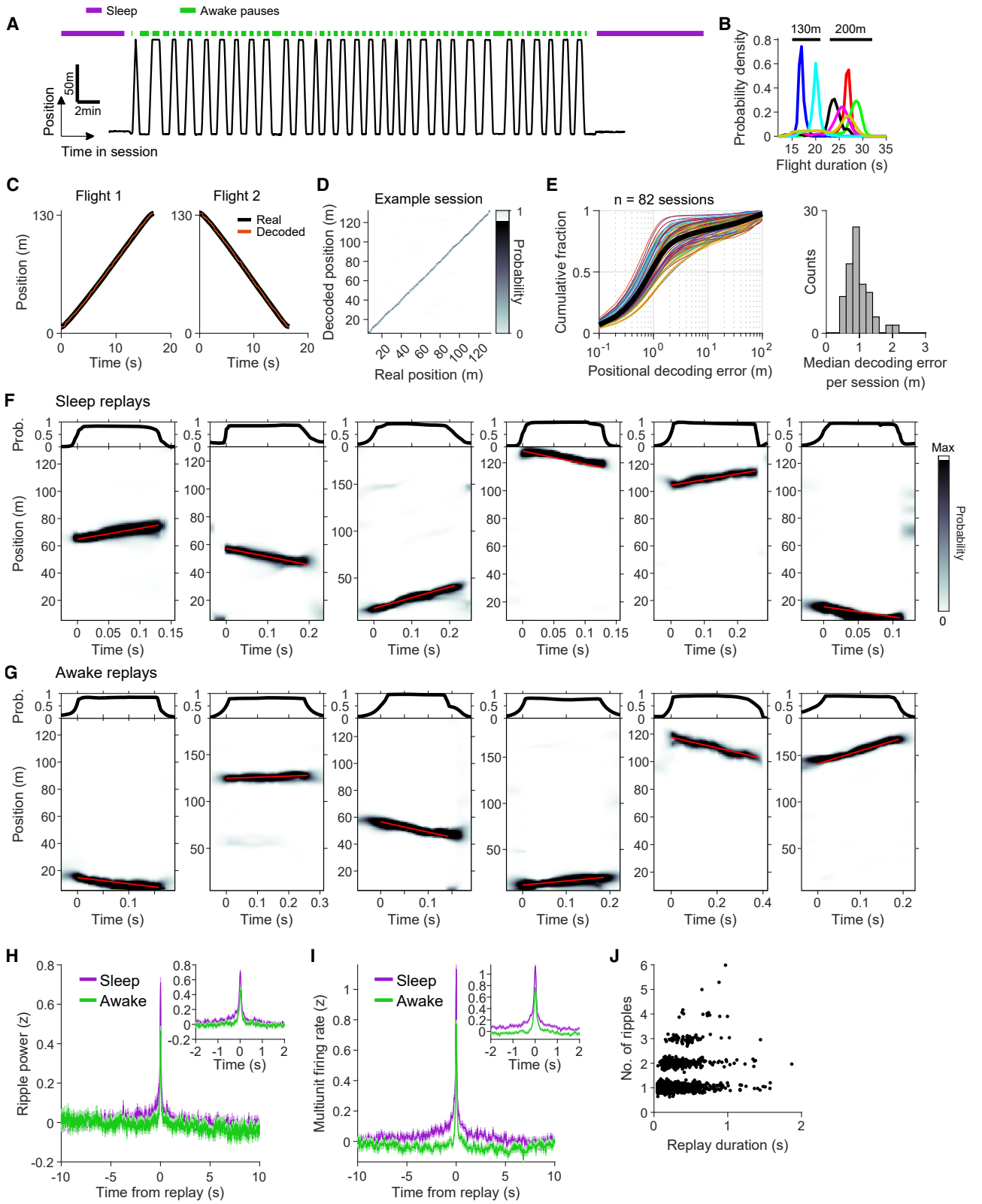

(legend on next page)

which were flying back-and-forth between two landing platforms in a 200-m-long or 130-m-long tunnel[29] (Figure 1A; localization accuracy 9 cm). Flight speeds were between ~6 and 8 m/s: the speed for each bat was very constant along the tunnel and was stable throughout each session.[29] Because of the considerable length of the tunnel, the durations of continuous flight epochs were very long: ~22–32 s in each direction for the 200-m tunnel and ~15–22 s for the 130-m tunnel (Figure 1B). Thus, both the spatial *size* of the environment and the temporal *duration* of continuous movement trajectories were much larger than in previous studies of hippocampal replay.

We used a multi-tetrode microdrive and a lightweight wireless neural-logger device to record neuronal ensembles from dorsal hippocampal area CA1 during *flight*[29] as well as during two offline states: (1) *awake* pauses between flights, wherein the bat paused on the landing platforms (median pause duration: 25.6 s) and (2) *sleep* sessions before and after the behavioral session (Figure 1A; STAR Methods). We used a clusterless state-space decoder[13,30] (STAR Methods) to decode the animal's position from the ensemble neuronal activity—both during behavior (flight decoding) and during sleep and awake pauses (replay decoding). We decoded position separately for the two flight directions because place-cell maps are independent between two movement directions.[29,31] The decoder's performance during flight was very good, with small decoding errors (examples: Figures 1C and 1D; population: Figure 1E). We retained for analysis 82 sessions for which the median decoding error during flight was low—less than 2% of the environment size—i.e., sessions that yielded high decoding accuracy (Figure 1E). For these sessions, the median decoding error was typically ~1 m, namely ~0.5% of the environment size (Figure 1E, right). In some sessions, the decoding error was even lower—as low as 0.5 m or 0.25% of the environment size. This extremely good performance of the decoder allowed us next to use the same decoder on the same 82 sessions in order to also decode neuronal activity during sleep and awake pauses—in search of replays.

Replays were readily observed during both sleep sessions and awake pauses (Figures 1F, 1G, S1, and S2; red lines are linear fits). Replays were defined using four criteria (STAR Methods): (1) decoder probability of being in a movement state: $p > 0.8$ (same threshold as in Gillespie et al.[13] and Denovellis et al.[30]), (2) replay score > 0.5, (3) replay duration > 50 ms, and (4) replay distance > 3 m (3 bins of 1 m). As in rodents, the replays typically occurred during sharp-wave ripple events in the local field potential (Figures 1H and S2A ["ripple"]) and were accompanied by an increase in the population firing rate (Figures 1I and S2A, top). Individual replays could span several sharp-wave ripples (Figure 1J), as shown previously in rodents.[28] Overall, we identified 7,213 replays from 82 sessions in 7 bats (3,663 sleep replays and 3,550 awake replays). This demonstrates that there are indeed hippocampal replays in ultra-large environments with a naturalistic spatial scale.

The spiking of individual neurons during replays reflected the neuron's multi-field tuning

In a previous study, we showed that hippocampal CA1 place cells exhibited multiple place fields as bats flew in the long tunnel.[29] This raised the following question: does the same neuron participate multiple times in each replay—once for each of its fields?

First, we observed that, in many cases, the spiking of individual neurons during replays indeed followed the spatial structure of their multi-field tuning (Figures 2A–2C; note that in Figure 2C middle, during the replay [red diagonal line], each of the neurons fired according to its tuning [which is shown on the right]; in particular, the green neuron fired twice in its two place fields

Figure 1. Behavior and examples of hippocampal replays in a very large environment

(A) Behavior of a bat in one example session (130-m tunnel). Black line, bat position versus time, showing its flights between the two ends of the tunnel. Purple horizontal lines, sleep sessions during which sleep replays were decoded. Green horizontal lines, awake-pause periods on the landing platforms, during which awake replays were decoded.

(B) Distributions of flight durations (for individual continuous nonstop flights in one direction). Colors, different bats. The different flight durations are due to flight-speed differences between individual bats, and to the two tunnel lengths (200 m: 5 bats, 130 m: 2 bats).

(C–E) Decoding position during flight behavior. (C) Examples of decoding for two individual flights, showing the real position (thick black line) and decoded position (thin orange line) versus time. (D) Confusion matrix of decoded position versus real position for the example session shown in (A) and (C). Grayscale, decoded probability; each column (1-m bins) depicts the probability-distribution that the bat was in that position; the sum of each column is 1. Note the high probabilities (dark-gray) along the diagonal, indicating excellent decoding during flight. (E) Population summary of decoder performance during flight. Left, cumulative distribution functions of the positional decoding error (absolute difference between bat's real position and the peak of the decoded posterior probability distribution). Colored lines, individual sessions (recording days) that passed the inclusion criteria of high decoding quality in flight ($n = 82$ sessions from 7 bats); black thick line, average of colored lines. Right, distribution of median decoding errors per session ($n = 82$ sessions).

(F) Examples of replay events during sleep. Top, posterior probability for the movement state in the decoder (marginal of the plot below); note the probability reaches values close to 1; we used a threshold of probability >0.8 for detecting replays. Bottom, decoded positions (posterior probability) versus time for the movement state (for display purposes, the colors in this 2D matrix were clipped between 1% and 99% percentiles of the probability values in the matrix). Overlaid red line, detected replay (based on Radon transform); time 0, start of detected replay.

(G) Examples of replay events during awake pauses. Plotted as in (F).

(H) Average ripple-power triggered on replay events, shown for ±10-s window around the replay event (time 0, replay centers; power Z scored separately for each ±10-s window)—plotted separately for sleep replays (purple, $n = 3,663$) and awake replays (green, $n = 3,550$). Shaded area, mean ± SEM. Inset, ±2-s zoom-in.

(I) Multiunit firing rate (Z scored), triggered on replay events; plotted similarly to (H). Note the increase in ripple power (H) and multiunit firing rate (I) around the decoded replay events.

(J) Replays could span several sharp-wave ripples, and the number of spanned sharp-wave ripples increased with the replay duration (Spearman $\rho = 0.33$, $p = 2.8 \times 10^{-61}$; data pooled for awake and sleep replays; shown only replays where ≥1 sharp-wave ripple was detected; data were jittered along the y axis for visualization only).

See also Figures S1 and S2.

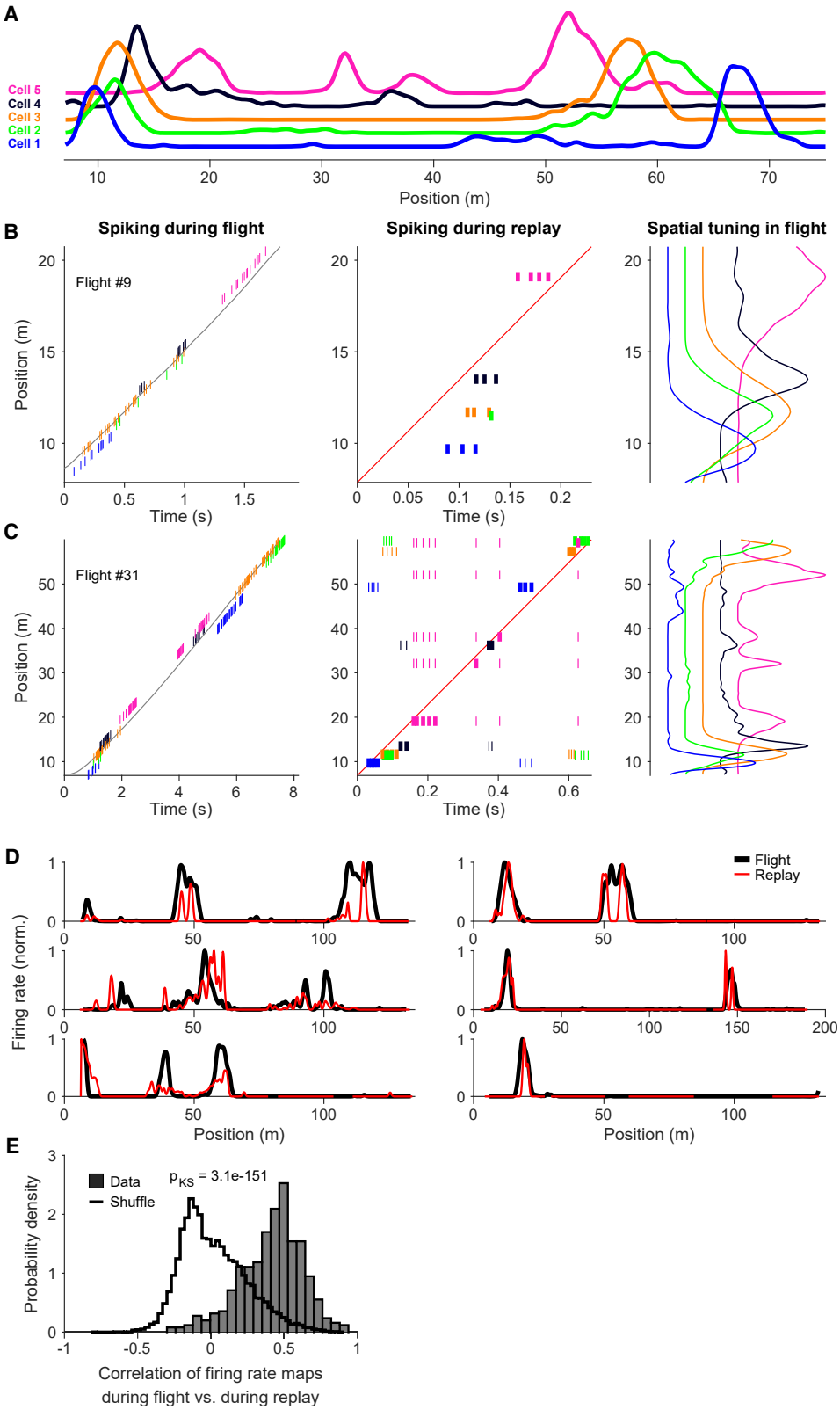

(legend on next page)

and likewise for the blue, orange, and black neurons; the pink neuron fired 4 times, in 4 of its 5 fields).

Second, we constructed within-replay tuning curves for individual neurons. These were computed similarly to the standard in-flight tuning curves—where spikes are counted in each position during flight and are then normalized by the time spent by the bat in that position during flight, pooling over all the flights in the session (Figure 2D, black curves)—but here, we counted the spikes in each *decoded* position during replays and then normalized them by the time spent in that *decoded* position during all replays in that session (Figure 2D, red curves; STAR Methods; we included here both awake replays and sleep replays). We found a striking similarity between the within-replay tuning curves and the standard in-flight tuning curves of the same neurons (examples: Figure 2D, compare red and black curves; population: Figure 2E, note the high correlations between the red and black curves for the real neurons ["data," gray bars] as compared with cell shuffles [black line]: t test of data versus shuffles, $p = 1.9 \times 10^{-278}$; Kolmogorov-Smirnov test, $p = 3.1 \times 10^{-151}$). This demonstrates again that the spiking of individual neurons during replays recapitulated the multi-field structure of their spatial tuning curves.

Replays were fragmented and encoded short snippets of the environment

Next, we investigated the properties of the replays. In rodents running in small environments, replays typically last between 100 ms and a few hundred milliseconds, they sweep at speeds that are usually between ~5- and 15-fold faster than the behavioral running speed of the animal, and an individual replay typically traverses most of the environment or the entire environment.[10–12,28,32] Here, we examined this in bats in the long tunnel. We used a standard method (based on the Radon transform; STAR Methods) to fit straight lines to the replay's decoded probability versus time (Figures 1F and 1G, red lines)—which allowed us to extract the replay's temporal duration, speed, and distance. We posited three distinct hypotheses on how the hippocampus may replay such a huge environment: (1) the replay durations would typically be 100–200 ms, similar to replay durations in rodents in small environments,[11,12,28] and the replay distances would span the entire tunnel length—but this will necessitate the replay *speed* to be extremely fast, ~1–2 km/s. (2) The replay distances would span the entire tunnel length, while the replay speeds would be only several-fold faster than the movement speed, similar to rodents in small environments[10,32]—but this will necessitate the replay *durations* to be extremely long: several seconds. (3) The replay duration would be similar to small environments, and the reply speed would be similar to small environments—but this will necessitate the replay *distances* to be extremely short, depicting very short fragments of the tunnel length. Of course, we might reveal some combination of these three hypotheses.

We found that replay duration had a broad distribution, with a median duration of 210 ms (Figure 3A)—similar to the distribution of replay durations in rodents in small environments.[10–12,30] Replay speeds (the slope of the red lines in Figures 1F and 1G) were broadly distributed up to ~150 m/s (Figure S3A)—much faster than replay speeds in rodents in small environments, which are typically 5–10 m/s.[10,32] Interestingly, replay speeds were correlated with the flight speed in the session (Figure S3B). Because the flight speed of bats in the tunnel was typically ~7 m/s (Figures S3C and S3D)—much faster than the running speed of rodents—we reasoned that it is problematic to directly compare replay speeds between species. Instead, we computed for each replay its "compression ratio": the ratio between the replay speed and the median flight speed in that session. This metric is normalized by the movement speed, and hence it allows direct comparison between bats and rodents. We found that the compression ratios were broadly distributed between 1 and 20, with a median compression ratio of 6.4 (Figure 3B)—similar to compression ratios for replays in rodents in small environments.[10] Thus, in this ultra-large environment, both replay durations and compression ratios for speed were similar to previous findings in small environments. This rules out hypotheses (1) and (2) above.

Next, we examined replay distances. Surprisingly, the replays spanned relatively short distances, typically between 5 and 20 m, with a median replay distance of ~8.1 m (Figure 3C). When normalized to the environment size, the median replay distance was 6.2% (Figure 3D)—a tiny fraction of the environment size: very different from previous results on replay in small environments, which typically cover most or all of the environment.

Figure 2. Spiking of individual neurons during replays reflected the neuron's multi-field tuning

(A–C) Example firing-rate maps of 5 neurons (A) and their spiking during individual flights and replays (B and C). (A) Spatial tuning curves (firing-rate maps) of 5 well-isolated simultaneously recorded neurons, ordered by the position of their first place field (tuning curves are for the same flight direction, and are shown only for a portion of the long tunnel). (B) Left, example spiking of these 5 neurons during one flight (the flight was in the same direction for which the 5 maps were computed; for visualization, the spikes of these 5 neurons were shifted up/down). Middle, spiking of these 5 neurons during one replay event; red line, replayed position versus time (the line fitted using the Radon transform, as the red lines in Figures 1F and 1G). Right, spatial tuning curves of the 5 neurons, zooming-in on the same range of positions as in the left and middle panels. Note that the 5 neurons fired sequentially along this replay according to the spatial positions of their place fields. (C) Another example of the spiking of the same 5 neurons during another flight (left) and another replay event (middle): this replay is longer than in (B). In (B) and (C) (middle), for every spike emitted by a neuron, we marked spikes (colored ticks) in all positions of all its place fields; the spikes closest to the replay position (red line) were marked in bold. Note that during the replay in (C), each of the 5 neurons fired according to its tuning: the green neuron fired twice, in its two fields, and likewise for the blue, orange, and black neurons; the pink neuron fired 4 times, in 4 of its 5 fields.

(D and E) Within-replay tuning curves for individual neurons were similar to their standard in-flight tuning curves. (D) Examples of 6 neurons, showing their standard in-flight tuning curves (black) and within-replay tuning curves (red). Note the high similarity of the black and red tuning curves. (E) Population histogram of the Spearman correlations between the within-replay tuning curves and in-flight tuning curves (correlation of the red and black curves in D) for the real neurons (gray bars, "data") and for cell shuffles (black line: correlations of in-flight tuning curve of neuron i and within-replay tuning curve of neuron j, for $i \neq j$, for all neurons from the same bat and same direction). Note the high correlations in the data compared with shuffles (Kolmogorov-Smirnov test: $p = 3.1 \times 10^{-151}$; t test: $p = 1.9 \times 10^{-278}$)—demonstrating that the spiking of individual neurons during replays reflected the multi-field structure of their tuning curves.

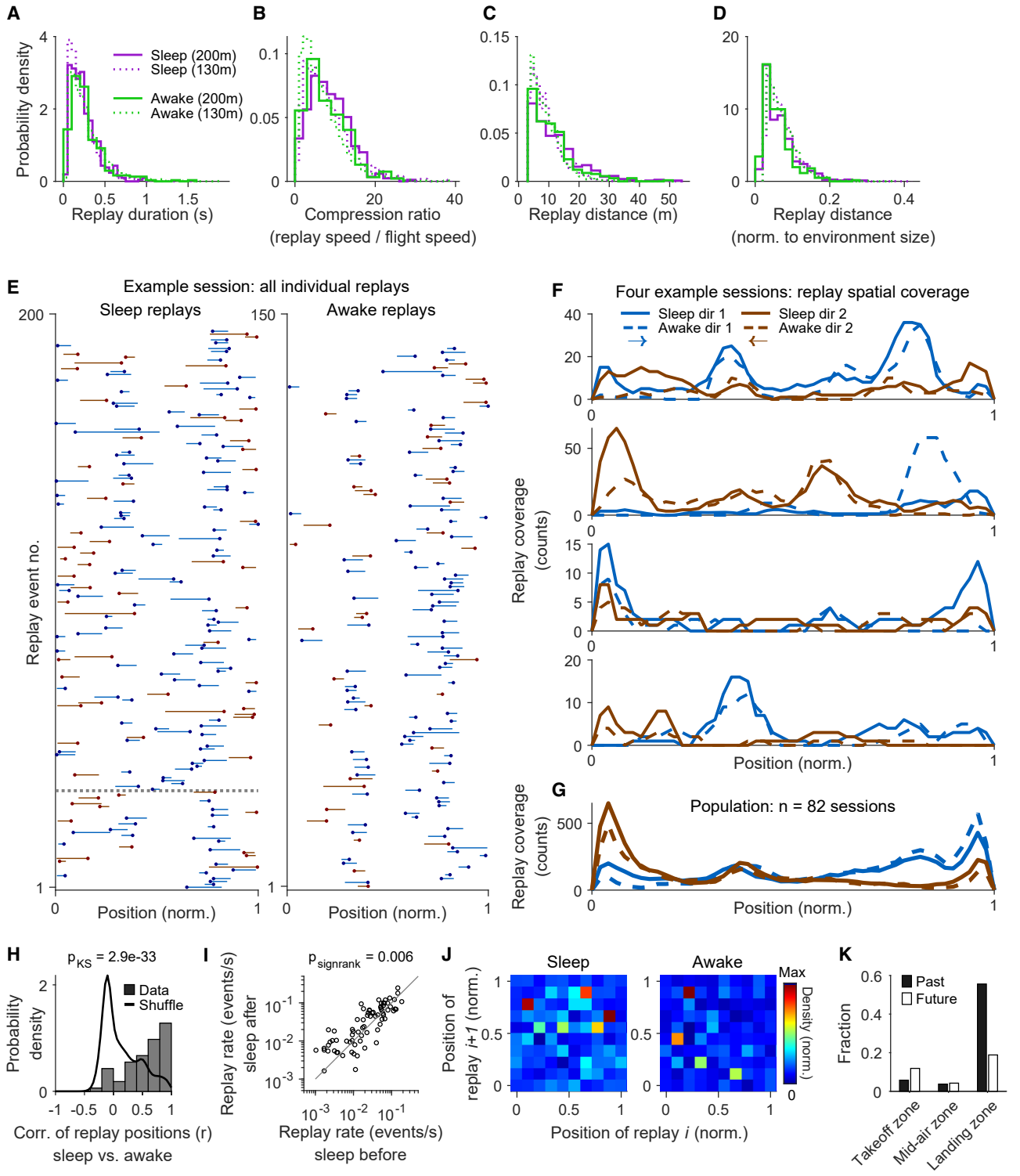

Figure 3. Fragmented replays depicted snippets of long experiences in the large environment

(A–D) Distributions of replay duration (A), compression ratio for replay speed (B), replay distance (C), and replay distance as a fraction of the tunnel length (D)—plotted separately for sleep replays (purple) and awake replays (green) for the 200-m tunnel (solid lines) and 130-m tunnel (dotted lines).

(E) Example session: awake replays (right) and sleep replays (left; dotted gray line separates sleep-before versus sleep-after behavior). Shown are individual replay positions (*x* axis, position normalized by tunnel length) along the session (*y* axis). Dots and lines show extent of individual replays (dot, replay start; tip of line, replay end); colors, map of flight direction from which the replay was decoded (same colors as in F and G).

(legend continued on next page)

We note that the bats' flight trajectories were long, with the bats flying continuously from one end of the tunnel to the other end (Figure 1A)—while the fragmented replays depicted only a tiny fraction of these continuous movement trajectories (Figure S3G). Taken together, the results shown in Figures 3A–3D support hypothesis (3) above: the replay durations and compression ratios for speed are similar to small environments—but the replay distances are extremely short, depicting very small fragments of this ultra-large environment. These findings were consistent across all 7 individual bats (Figures S4A–S4D); we note that in another (8th) bat, which performed a more demanding task than our standard back-and-forth shuttling task, we observed slightly longer replays: see Figure S5, and this may suggest that replay distances can become more prolonged under more demanding tasks. Further, we found that similar fragmented replays existed already in the first few days (sessions) of exposure to the large environment (Figures S6A and S6B)—consistent with our previous finding that the properties of the neural code for space were stable across days, from the very first day.[29]

We next asked which positions along the tunnel were represented by the replays. We found that replay positions were not distributed uniformly along the tunnel (Figures 3E–3G). In particular, replays represented more often the landing/takeoff locations at the two ends of the tunnel (Figures 3G and S4E). Furthermore, there was also a non-uniform representation in the central portion of the tunnel (Figures 3E–3G). This was the case even though the firing rate of the multiunit data used in the clusterless decoder was distributed uniformly along the tunnel on all days (Figures S6C and S6D; note there was a higher firing rate at the two ends of the tunnel; we also note that there could be some non-uniform distribution of place fields in the population of neurons sampled by our recordings, which might lead to the non-uniform spatial distribution of replay positions). Moreover, the distributions of replay positions tended to change from day to day (Figure 3F, top three examples depict different sessions from the same bat). However, within-day the replay positions were stable along the session (Figure 3E) and were similar between sleep replays and awake replays (examples: Figure 3F; population: Figure 3H). This similarity between sleep and awake was driven mostly by the sleep after the behavioral session because the replay rate was significantly higher during sleep after the session compared with sleep before the session (Figure 3I; median ratio of replay rate in sleep after/before: 1.4; Wilcoxon signed-rank test: $p = 0.006$). These results might reflect day-to-day changes in hippocampal network internal dynamics[33] or changes in behavioral relevance: for example, the bat may attend to one set of locations on one day but to another set of locations on another day—and this may explain the across-day variation but within-day similarity between the sleep and awake distributions of replays. Although the replay positions showed some within-day consistency over the hour-long timescale of a session (Figure 3E), they did not show any clear regularity on shorter timescales: the positions of two consecutive replays were generally uncorrelated and did not show any clear pattern (Figure 3J, there is no over-representation of the diagonal). This latter result also argues against the possibilities that (1) very long replays do exist (long in both time and distance) but were potentially cut to pieces by our detection algorithm or (2) long replays are composed of trains of "mini replays," wherein each mini replay continues where the previous one has ended—because if either of these options were true, we would expect to see sequential dependencies between consecutive replays, with clear structure on the diagonal or parallel to the diagonal in Figure 3J. However, this was not the case in the data (Figure 3J).

Finally, for the awake replays, we asked whether they predominantly represent past trajectories or future trajectories. This can be addressed because hippocampal place cells are known to exhibit different maps for the two movement directions[31]—and this was also the case in the tunnel.[29] By examining which of these two spatial maps (which of the two directions) the replay belonged to, we could assign whether the replay represented the *immediate past* (the map direction in which the bat had just flown) or represented the *immediate future* (the map direction in which the bat will fly next). We found that replays represented both past and future, but there was a larger prevalence of replays representing the past (Figures 3K and S7B)—consistent with previous findings on replays in rodents in 1D small environments, which reported more past replays,[12,13] and in line with the

(F) Spatial coverage of replays for 4 example sessions (4 panels). Shown are the distributions of replay positions (spatial coverage) along the tunnel, separately for the two directions (two colors), for sleep (solid lines) and awake (dashed lines); *x* axis, position normalized by tunnel length. Each replay contributed to the distribution at all spatial bins covered by the replay. Top, example session from (E).

(G) Population distributions of replay positions along the tunnel ($n = 82$ sessions), plotted as in (F).

(H) Gray histogram, Pearson correlations of the distributions of replay positions in sleep versus awake (e.g., correlation of solid versus dashed lines in F), for the same direction, pooled across sessions and directions ($n = 164$). Black line, histogram for session-shuffles: correlations for sleep in session i versus awake in session j for $i \neq j$ (for same direction). Kolmogorov-Smirnov test (data versus shuffles): $p = 2.9 \times 10^{-33}$.

(I) Scatter of replay rate in the sleep session after behavior versus sleep session before behavior. The replay rate was higher in sleep-after than in sleep-before behavior (Wilcoxon signed-rank test: $p = 0.006$; $n = 82$ sessions).

(J) Population average 2D distribution of positions of consecutive replays (position of replay $i + 1$ versus position of replay i), plotted separately for sleep replays (left) and awake replays (right); $n = 82$ sessions. To factor out the per-day distribution of replay positions, we normalized the 2D distribution of replay positions for each session by its marginal 1D distribution, prior to averaging across days (the averaging was weighted by the number of replays in each session).

(K) Number of replays that represented past (black) and future (white) for different replay locations in the tunnel: takeoff zone (the first 5% portion of the tunnel in each map direction), mid-air zone (the 90% central portion of the tunnel), and landing zone (the last 5% portion of the tunnel in each map direction). Fractions were normalized by the relative portions of takeoff/mid-air/landing zones (normalized via dividing by 0.05/0.90/0.05 and then normalizing the sum of all bars to 1; for unnormalized fractions, see Figure S7A; for further sub-division to forward and reverse replays, see Figure S7D). "Past" and "future" refer to the immediate past (the map corresponding to the immediately preceding flight) and immediate future (the map corresponding to the immediately following flight). Note the prevalence of replays representing past landing (large black bar).

See also Figures S3–S7.

proposed role of replays in memory. In particular, replays strongly represented past landing events (Figure 3K, "landing zone"—black bar; binomial test of past versus future for the landing zone: $p = 3.4 \times 10^{-64}$; past landing refers to replays that occurred near the current awake-pause platform of the bat, in the map direction corresponding to the past flight toward that platform; see also Figure S7D). The prevalence of replays for past landing can also be seen in Figure 3G (note the blue histograms are higher in the right platform and the brown histograms are higher in the left platform). This over-representation of past landings by hippocampal replays might possibly arise because landing is associated with reward (arriving at a rewarded location) and with high attention and high difficulty (as landing is a challenging motor maneuver). Interestingly, for takeoffs, replays represented the future more strongly than the past (Figure 3K, "takeoff zone"—white bar is higher; binomial test of future versus past for the takeoff zone: $p = 1.8 \times 10^{-8}$). This suggests a predominantly future-*planning* role for takeoff replays versus a predominantly past-*memory* role for landing replays. It may also suggest a role for the temporal proximity between the replay and the recently occurred/soon-upcoming behavioral events. Further, we found a larger fraction of forward replays than reverse replays (Figure S7C; "forward" replays denote that the replay direction corresponds to the flight direction of the spatial map from which the replay was decoded, and "reverse" replays are when the direction is opposite; see also Figures S7F and S7G)—again, consistent with previous findings on replays in rodents in 1D small environments, which reported a larger prevalence of forward replays.[12,28,34]

Overall, most properties of replays in this ultra-large environment were similar to previous studies in small environments in rodents: (1) replays co-occurred with sharp-wave ripples and with population bursts, (2) replays had similar durations as in small environments and (3) similar speed compression ratios, (4) replays represented the past more than the future, and (5) there were more forward replays than reverse replays. However, there was one major difference from previous studies in small environments: the replays in this huge environment were highly fragmented and covered short distances, which constituted a tiny fraction of the environment size: typically, only ~6% of the tunnel length.

Replays in a smaller 15-m tunnel covered a much larger fraction of the environment

We next set out to test whether, in small environments, replays in bats cover a *larger* fraction of the environment size than we found here in the long tunnel. In other words, we asked whether, in small environments, replays behave similarly in bats and rodents. To address this, we conducted recordings in dorsal CA1 of an additional bat that was flying in a short, 15-m portion of the tunnel (blocked by curtains). As before, we were able to faithfully decode the bat's position when it was flying (Figures 4A and 4B). We then examined the sleep sessions and the periods of awake pauses on the landing platforms. We used the same clusterless decoding algorithm as before—and found many replays during sleep and awake (examples: Figure 4C; we detected 345 replays in 6 recording sessions). Many of these replays spanned a large fraction of this environment (Figure 4C)—which was *never* observed in the long tunnel. When comparing quantitatively the replays between the short 15-m tunnel and the long tunnel, we found that the replay duration was smaller in the short tunnel (Figure 4D, leftmost), the speed compression ratio was similar between the two tunnels (Figure 4D, second), and, importantly, the normalized replay distance—measured as a fraction of the environment size—was much longer in the short 15-m tunnel as compared with the long tunnel (Figure 4D, rightmost; see also Figure 4E). In particular, in the 15-m tunnel, about a quarter of the replays exhibited replay distances >30% of the environment size (Figure 4D, rightmost, black boxplot: top of inter-quartile box [75%])—whereas in the long tunnel we *never* observed such long replays. The median replay distance in the 15-m tunnel was 21% of the environment size, whereas in the long tunnel the median distance was 6.2%—namely, 3.4-fold shorter. Further, in the long tunnel, only 1% of the replays were longer than 21% of the environment size (Figure 3D), while in the 15-m short tunnel, 50% of the replays were longer than 21% of the environment size (Figure 4D, rightmost, black boxplot [see the median]; see also Figure 4E, leftmost violin distribution). We note that the replay distances in the short 15-m tunnel are still much less than 100% of the environment (Figure 4E); however, because 15 m is not truly a "small environment," we anticipate that the fraction of the environment covered by replays will increase even further as the environment size decreases. Taken together, we found here that in a smaller environment (15 m), replays often covered a substantial portion of the environment—akin to previous findings in rodents running on small tracks.

Replays carried behaviorally relevant information

The results presented so far have already indicated that replays are related to the bat's behavior: this was suggested by the over-representation of replays for past landings and for future takeoffs (Figure 3K: landing zone, black bar; takeoff zone, white bar)—reflecting an asymmetry in replays for past versus future. Here, we searched for further evidence supporting the idea that replays carry behaviorally relevant information.

We started off by searching for other types of asymmetries in replays. We observed remarkable directionality of replays in some of the sessions (Figures 5A, 5B, and S8A). Although in most sessions the replays pointed equally in both directions (Figure 5B, replay directionality index ~0, reflecting symmetry), we observed in a few sessions a highly significant fraction of replays that pointed in the same direction—either toward the exit door from the tunnel (example session: Figure 5A; see Figure 5B, leftmost arrowhead) or away from the exit door (the other 3 arrowheads in Figure 5B). This unexpected asymmetry cannot stem from the decoding method because this method is symmetrical, so there is no reason *a priori* to expect such a strong replay asymmetry. Interestingly, the door is very behaviorally relevant because this is the location where the bat was released and where the experimenter was sitting throughout the session—and the door also denotes the potential "escape direction" from the tunnel. The direction away from the exit door, on the other hand, is the direction away from the experimenter. We speculate that the high asymmetry of replay directions in these sessions may reflect

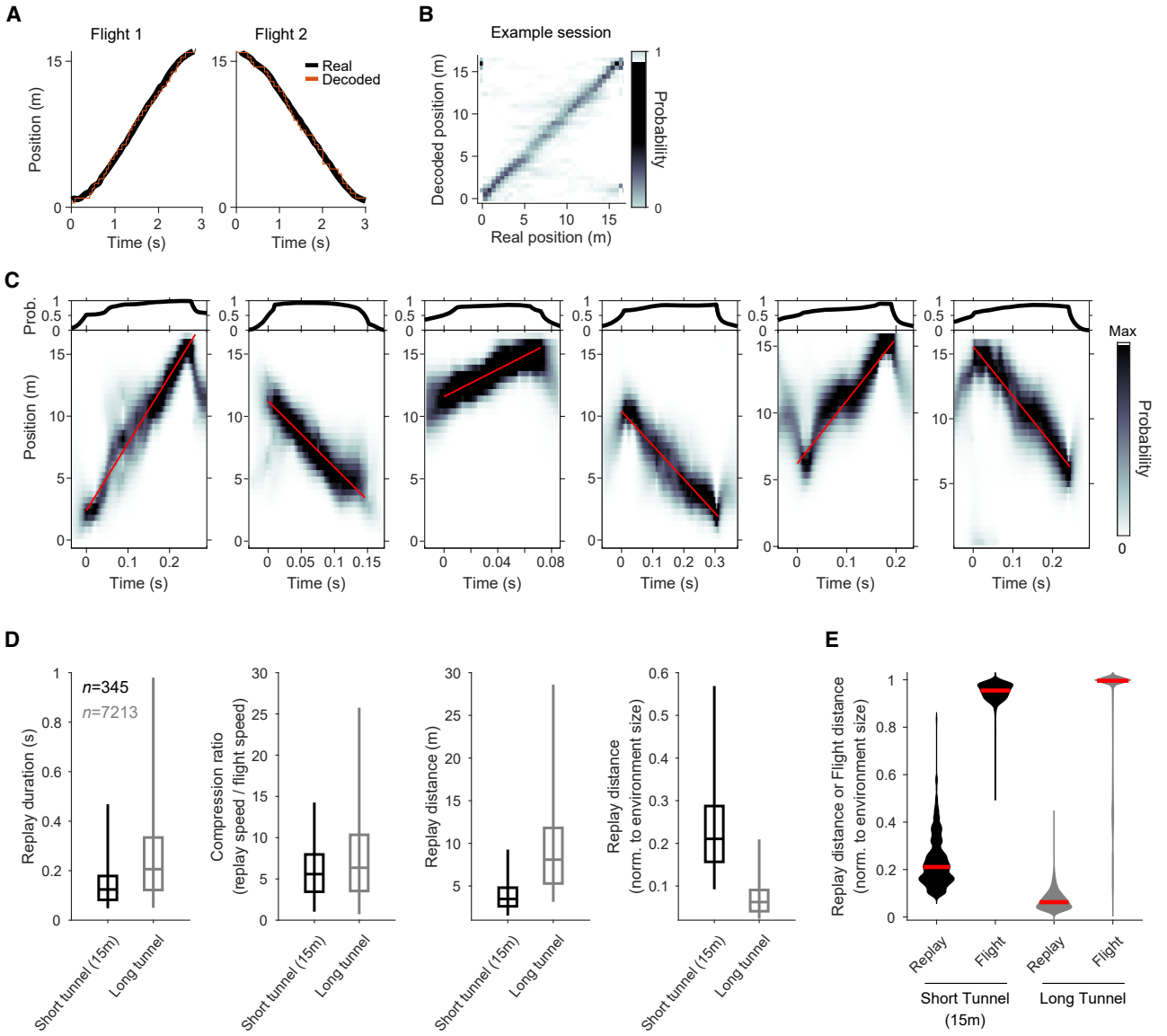

Figure 4. Replays in a smaller tunnel covered a much larger fraction of the environment

Data from one bat that was flying in a short 15-m tunnel.

(A and B) Decoding of position during flight behavior. (A) Examples of decoding for two individual flights; plotted as in Figure 1C. (B) Confusion matrix of decoded position versus real position for one example session; plotted as in Figure 1D. Note the high probabilities along the diagonal, indicating very good decoding during flight.

(C) Examples of replay events during sleep and during awake pauses; plotted as in Figures 1F and 1G. Note that these replays covered a much larger fraction of the environment than replays in the long tunnel.

(D) Comparison between the short 15-m tunnel (black boxplots) and long tunnel (gray boxplots) for the following replay parameters: replay duration (leftmost), compression ratio for replay speed (second), replay distance (third), and replay distance as a fraction of the tunnel length (rightmost). Data pooled over sleep replays and awake replays. Boxplots show the median (horizontal line), 25%–75% percentiles (boxes) and 1%–99% percentiles (whiskers).

(E) Distributions of replay distance and flight distance, normalized to the environment size, plotted separately for the short 15-m tunnel (left two distributions) and for the long tunnel (right two distributions). These distributions are kernel density estimates (smoothed) and are plotted as violin plots; red line, median; data pooled over sleep replays and awake replays. Note that the bats exhibited continuous nonstop flights from one end of the tunnel to the other, yet the replays were highly fragmented.

the bat's behavioral preferences, attention, or other cognitive factors.

Next, we analyzed data from a different set of experiments, where pairs of bats flew toward each other in a 135-m tunnel and were crossing over each other in opposite directions[35] (Figures 5C and 5D). These crossings-over were highly salient events that required collision avoidance, and they were accompanied by increased echolocation and attention levels.[35] We recorded neuronal data from one bat in each pair in this experiment. In one such bat, we have recorded sufficiently large

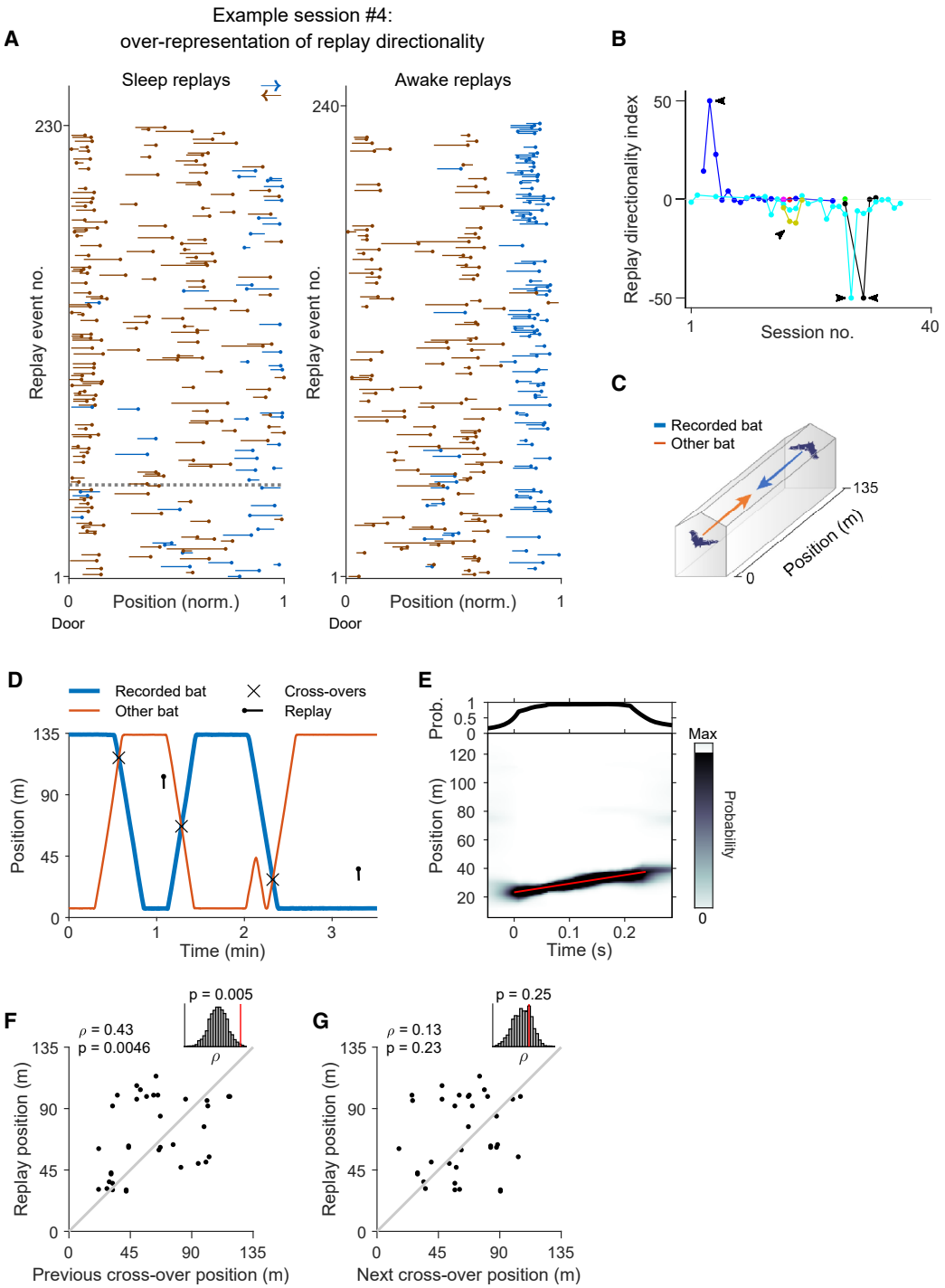

Figure 5. Fragmented replays carried behaviorally relevant information

(A and B) Directionality of replays. (A) Example of a session where replays showed high directionality, with most replays pointing in one direction—the direction of the exit door from the tunnel. Arrows indicate map direction. Plotted as in Figure 3E. (B) Replay directionality index for all the sessions in which ≥20 replays were detected (dots, sessions; colors, individual bats [same colors as Figure 1B]; we pooled sleep and awake replays). Replay directionality index = surprise of the *p* value of the binomial test comparing the number of replays pointing toward the tunnel door versus the opposite direction: surprise = $-\log_{10}$ (*p* value). Positive values, replays point toward tunnel door; negative values, away from tunnel door. *y* axis was clipped at ±50 for display purposes (surprise = 50 corresponds to *p* value = 10^{-50}). *x* axis shows recording session no. for each bat, from first exposure to the large environment (only two bats were recorded from first exposure [session 1], colored blue and light-blue; for the other bats, the first recording session was plotted based on number of preceding training sessions). Black

(legend continued on next page)

ensembles of hippocampal CA1 neurons to allow decoding of replays (Figures 5D and 5E; the same criteria for replay detection were applied here as in the main dataset, but here we removed replays near the platforms in order to focus on the replays that represented mid-air locations, where cross-overs occurred: STAR Methods). We found that also, in this dataset, replays were fragmented, depicting short distances (example: Figures 5E and S2H; population: Figures S4F–S4J). Interestingly, we found that the position of awake replays, which occurred while the bat was pausing on the platform, was correlated with the position of the last cross-over during flight (Figure 5F; Spearman $\rho = 0.43$, $p = 0.0046$; comparison to random permutations [inset]: $p = 0.005$). The same result was found also when considering only those replays that belonged to the map corresponding to the bat's flight direction during the cross-over (Figure S8B). This suggests that awake replays tend to recapitulate the position of the recent highly salient behavioral event—the cross-over with the other bat. As a control, we also computed the correlation between the positions of replays and the *next* cross-over position during flight—where we expect to see no correlation because the next cross-over position cannot be readily predicted by the bat while it pauses on the platform. Indeed, we found no such correlation (Figure 5G; Spearman $\rho = 0.13$, $p = 0.23$). There was also no correlation between replay position and 2-back or 3-back cross-over positions (Figures S8D and S8E). Overall, the results of the two-bat experiment demonstrated that the short replay snippets, which we found in the hippocampus of bats flying in this huge environment, carried behaviorally relevant information about salient past behavioral events.

DISCUSSION

Previous studies of hippocampal sequential replays were typically conducted in small laboratory environments and were limited to investigations of rodents. Here, we studied hippocampal sequential replay in flying mammals—bats—which were flying in an ultra-large environment: a 200-m tunnel. We found sequential replays—which is a nontrivial finding because, in this tunnel, CA1 place cells exhibit a multi-field spatial code,[29] possibly making it more difficult to generate replays. Individual neurons fired according to their multi-field spatial tuning, wherein the same neuron could fire multiple times within the same replay, according to the spatial locations of its multiple fields (Figure 2). Importantly, these replays carried behaviorally relevant information about past behavioral events: both about past landings on the platforms, where reward is given (Figure 3K, landing zone—black bar) and about past events of cross-overs with another bat (Figure 5F). The replays also predominantly represented past flights as compared with future flights—in line with the proposed role of hippocampal replays in memory.[10–15,18–21] These replays had similar temporal durations as in small environments in rodents and similar speed compression ratios—suggesting that, across species, there are some conserved mechanisms of hippocampal replay or conserved computational constraints. However, *unlike* previous studies in small environments in rodents, the replays in this very large environment were highly fragmented and covered relatively short distances, which constituted on average only ~6% of the environment size. Thus, these replays depicted very short snippets of long experiences.

This dramatic difference was not due to the *species* difference between bats and rodents—because in a bat flying in a much smaller environment (15-m tunnel), the replay distance covered a much larger fraction of the environment size (Figure 4). It was also likely not due to the *speed* difference between bats and rodents—because the bat's flight speed was only slightly higher in the long tunnel versus the short 15-m tunnel: for the one bat in which we recorded in both the long tunnel and the short 15-m tunnel, the median flight speeds was 9.8 and 7.1 m/s, respectively (median of the peak speeds per flight)—a 1.38-fold ratio. This cannot explain the 3.4-fold longer replay distance (as a fraction of tunnel length) that we found in the small environment (Figure 4). Thus, we conclude that the ultra-short, fragmented replays that we found in the very large environment were due to the environment *size*. Consequently, we predict that in rodents fragmented hippocampal replays will also be found in very large, naturalistic environments. In other words, we posit that fragmented replays are the *norm*—across species—but this fragmentation cannot be uncovered in very small environments such as typical laboratory setups.

Our results are fundamentally different from a previous study,[28] which used a 10-m track and showed many long replays that covered a substantial fraction of the track and often the entire track. This was achieved by replaying trajectories coherently across several sharp-wave ripples. Here, we also found that individual replay snippets could continue across several sharp-wave ripples (Figure 1J). However, crucially, we discovered here that in a much-larger 200-m environment, replays covered a tiny fraction of the track—on average only 6.2% (Figure 3D). This result is in stark contrast to the previous study, and it suggests that there is a limit to how much replay distance can be increased by chaining the replay across

arrowheads denote 4 sessions, in 4 different bats, where replays exhibited strong directionality: leftmost arrowhead points to the session in (A), which exhibited high replay directionality toward the tunnel door; other 3 arrowheads: sessions with high replay directionality away from tunnel door.
(C–G) Fragmented replays in the two-bat experiment depicted behaviorally relevant cross-over events. (C) Experimental setup for two-bat experiment: the two bats flew in opposite directions and passed each other (cross-over). Neural data were recorded from one of the bats (blue arrow). (D) Example of 3.5-min of behavior during one session (blue and orange lines, positions of recorded bat and other bat; ×, cross-over events), and awake replays during pauses between flights (black dot-and-line symbols; dot, replay start; tip of line, replay end). (E) Example of awake replay in the two-bat experiment. Plotted as in Figures 1F and 1G. (F and G) Positions of replays (dots) versus the positions of the previous cross-overs (F) or next cross-overs (G). Data from one recorded-bat in the two-bat experiment ($n = 35$ significant awake replays from 5 sessions [one bat-pair]). Spearman correlations ρ are indicated. Insets, comparison of the real Spearman correlations ρ (red line) and the Spearman correlations for 1,000 random permutations of the dots (shuffles, gray histogram; in each shuffle we randomly permuted the dots' x values while keeping the same y values as in the original scatter). Above each inset we indicated the p value of data compared with shuffles.
See also Figure S8.

multiple sharp-wave ripples. Interestingly, in this previous study in rodents[28] there were also many replays that were short—covering around 20%–30% of the environment size. This partial fragmentation of the replays may potentially be explained by the fragmented behavior of the rats: in the 10-m track, the rats often stopped and then resumed running, exhibiting a "stop-and-go" behavior that could underlie the partial fragmentation of the replays. By contrast, in our experiments, the bats' behavior was continuous: they flew continuously from one end of the tunnel directly to the other end (see Figure 4E, long tunnel—"flight"; and Figure S3G, blue). Therefore, in our study, the fragmented replays (Figure 4E, long tunnel—replay; and Figure S3G, red) cannot be explained via fragmented behavior. Importantly, in the 15-m track, our bats also flew continuously from one side to the other—and yet the replays were less fragmented (Figure 4E, short tunnel: replay versus flight). Thus, what determines the difference in replay fragmentation between the long tunnel and the short 15-m tunnel is not a difference in the fragmentation of experience—because in both cases the experience was continuous—but rather the spatial scale of the environment. In other words, our study demonstrates that, in very large environments, the hippocampus exhibits fragmented replays of *continuous* experience.

Limitations of the study

One limitation of our study is that the task that we used was very simple: linear shuttling from one end of a tunnel to the other end. It is possible that replay distance would increase under more challenging tasks. It would therefore be interesting to design a more demanding task that requires remembering long portions of the environment and examine its impact on the replay distance. Second, to further support the behavioral relevance of the fragmented replays, it would be interesting in the future to perform systematic experimental manipulations: for example, one could introduce in the middle of the session a new reward location or a salient object in the center of the tunnel—and then examine whether the replays dynamically start to overrepresent these new important locations.

Mechanistic and functional implications of the fragmented replays

What are the implications of the fragmented replays that we found in this very large environment? We will discuss below two types of implications: (1) mechanistic implications (Marr's implementation level)—such as biophysical/network constraints on replay—and (2) computational or functional implications (Marr's computational/algorithmic levels)—such as chunking of memory or hippocampal-neocortical communication.

(1) *Mechanistic implications*. We hypothesize that there may be some *biophysical or network constraints* on the duration and speed of replays—which may explain why the durations and speed compression ratios are relatively conserved across small and large environments and across species. Thus, perhaps the hippocampus simply cannot generate replays that last several seconds—or several *minutes*, which is the replay duration that would be required in order to replay the continuous flights of bats outdoors, which may last >30 min.[36] Likewise, perhaps the hippocampus cannot generate ultra-fast replays with speeds of several km/s—or *hundreds* of km/s, which is the speed that would be required in order to replay within 100–200 ms the 30-km flights of bats outdoors.[36] These limitations could stem from recurrent dynamics in the CA3-CA1 network during sharp-wave ripples. Alternatively, they could stem from limitations on the speed of axonal or synaptic delays: in particular, because in this large environment the place-field sizes do not scale up linearly with the environments size.[29] This implies that replaying the entire large environment would require crossing many more place fields; this, in turn, would require activating more synapses—which may pose limits on replay speed. But, if there are such biophysical/network limitations on the duration and speed of replays, then this necessitates that for such a huge environment, the replay distances must be only a small fraction of the environment size.

(2) *Computational or functional implications*. We hypothesized two functional implications for the fragmented replays.

(i) *Chunking of memory*. The bats' flight episodes had long durations—around half a minute per flight (Figure 1B). We hypothesize that such long episodic events may require *chunking* of memory encoding—which is reflected by the observed piecewise replay. We propose that this piecewise replay of chunked information in the hippocampus is then being sent to the neocortex for memory consolidation. This notion is consistent with findings on chunking (fragmentation) of memory encoding in humans.[37–39] It is also consistent with the selective replay of important events that we observed in our data—e.g., landings (Figure 3K) and cross-overs between two bats (Figures 5C–5F)—because fMRI studies in humans showed strong hippocampal activation and memory reactivation of event boundaries, which, in turn, are related to chunking of memory.[38,40] We note that such chunking may be even more crucial for encoding natural flights outdoors, which can last dozens of minutes; in this case, chunking may be absolutely necessary. Another interpretation is that the fragmented replays reflect *selection* of particularly salient events for memory consolidation—or, alternatively, they reflect selective memory recall. This notion is consistent with the observed prevalence of replays representing past landing (Figure 3K), as well as with the relation of replay position to the position of previous cross-over with another bat (Figures 5C–5F). It can also explain why the spatial distribution of replay positions is non-uniform and differs across days: because in each day the hippocampus selectively consolidates (or recalls) memories about different salient events or different locations of interest.

(ii) *Hippocampal-neocortical communication*. As already discussed above, a prominent theory posits that hippocampal replay is a mechanism by which information is being sent from the hippocampus to the neocortex—either for memory storage or for future planning.[14,15,22–25] We hypothesize that this hippocampal-neocortical communication system may operate, at least in some aspects, analogously to artificial communication systems. Specifically, when a large message needs to be sent in artificial communication systems, such as the internet, this message is being cut to small pieces, called

packets. In our case, the large message to be sent is the long flight episode, and this message needs to be broken into smaller pieces—namely the fragmented replays. In other words, we speculate that the piecewise replay of information that we observed here might be akin to using small information packets for transmitting large messages in artificial communication systems—but here seen for the first time in the biological brain. In particular, the random order of replays (Figure 3J) is reminiscent of the seemingly random order of information packets that are sent in distributed artificial communication systems, such as file-sharing networks (e.g., BitTorrent)—where the main advantage of the seemingly random order of packets is enhanced robustness and fault tolerance. This possibility opens an important question for future research, namely how does the neocortex reassemble these fragmented pieces of information back into coherent messages? A related interpretation is that of *hippocampal training of neocortical networks*: namely, the neocortex stores a model of the world and hippocampal networks train neocortical networks by sending supervised information—a process sometimes called "systems consolidation" of memory.[2,25,41] Notably, in training algorithms of deep neural networks, it is well established that the best way to train is by using short snippets of information, called "mini-batches," as the use of mini-batches creates broad minima in the training functions that are easier to learn and generalize.[42–44] We hypothesize that, likewise, training of the neocortical network by the hippocampal network is being done by sending short snippets of long experiences via fragmented, piecewise replays.

In summary, our finding of highly fragmented, piecewise replays of ultra-long navigational trajectories opens new directions for future research. These findings highlight the importance of studying replay of longer experiences, in more ecological settings—such as in larger environments—in order to fully capture the naturalistic aspects of replay. Moreover, these surprising results call for re-thinking of ideas about hippocampal physiology and function—including hippocampal population dynamics, memory reactivation, consolidation, chunking, network training, and hippocampal-neocortical communication.

RESOURCE AVAILABILITY

Lead contact

Further information and requests for resources should be directed to the lead contact, Nachum Ulanovsky (nachum.ulanovsky@weizmann.ac.il).

Materials availability

This study did not generate new unique reagents.

Data and code availability

- Data reported in this paper are available from the lead contact upon request.
- All the behavioral and neural data in this study were analyzed using custom code written in MATLAB, and the state-space decoder analysis was performed in Python. The Python code package used for decoding was taken from Denovellis et al.[30] and can be found here: https://github.com/Eden-Kramer-Lab/replay_trajectory_classification. Original code used in this study has been deposited at Zenodo and is publicly available at DOI https://doi.org/10.5281/zenodo.15330798 as of the date of publication.
- Any additional information required to reanalyze the data reported in this work is available from the lead contact upon request.

ACKNOWLEDGMENTS

We thank A. Rubin, J. Aljadeff, I. Norman, I. Mashanova-Golikova, R. Yerushalmi, Y. Waserman, S. Ray, and G. Ginosar for comments on the manuscript; S. Futerman, I. Shulman, B. Pevzner, K. Dor, S. Kodenzik, E. Solomon, C. Cohen, A. Shalev, N. Raish, A. Zayarni, and L. Hartman for help with bat training and experiments; G. Ankaoua and B. Pasmantirer for mechanical designs; A. Tuval for veterinary support; and G. Brodsky for graphics. N.U. is the incumbent of the Barbara and Morris Levinson Professorial Chair in Brain Research. This study was supported by research grants to N.U. from the European Research Council (ERC-CoG – NATURAL_BAT_NAV), Deutsche Forschungsgemeinschaft (DFG – SFB 1372), Minerva Foundation (no. 714445), Dr. Lou Siminovitch Laboratory for Research in Neurobiology, Dorraine S. Schwartz, Debra and Paul Sagues, and Yehuda and Judith Bronicki; by research grants to N.U. and L.L. from the National Institutes of Health (NIH R01 – NS121413), CRCNS NSF-BSF (BSF 2020806), and Israel Science Foundation (ISF 1829/23); and by the André Deloro Prize for Scientific Research and the Kimmel Award for Innovative Investigation to N.U. T.E. was supported by the Otto Schwarz Scholarship, the Horowitz KKL-JNF Foundation, and the Maccabim Foundation Excellence Fellowship for PhD students.

AUTHOR CONTRIBUTIONS

T.E. and N.U. conceptualized this study. T.E., S.R.M., L.L., and N.U. set up experimental systems. T.E. and S.R.M. conducted the experiments in the long tunnel for the main dataset, S.R.M. conducted the experiments in the short tunnel, A.S. and S.P. conducted the experiments for the two-bat dataset. T.E. performed the data analysis, and S.R.M. contributed to the data analysis. N.U. guided the data analysis, with major inputs from L.L. T.E. and N.U. wrote the first draft of the manuscript, and all authors participated in writing and editing of the manuscript. N.U. supervised the project.

DECLARATION OF INTERESTS

The authors declare no competing interests.

STAR★METHODS

Detailed methods are provided in the online version of this paper and include the following:

- KEY RESOURCES TABLE
- EXPERIMENTAL MODEL AND STUDY PARTICIPANT DETAILS
  - Animals, behavior, and electrophysiological recordings
- METHOD DETAILS
  - Detecting multiunit spikes, and spike sorting of individual neurons
  - Clusterless state-space decoder
  - Quantifying decoding-accuracy, and inclusion criteria for sessions
  - Detecting replay events during sleep and awake
  - Quantifying replays, and inclusion criteria for replays
  - Computing firing-rates maps for individual neurons, in-flight and within-replays
  - Sharp-wave ripples, and multiunit activity
  - Data and code availability
- QUANTIFICATION AND STATISTICAL ANALYSIS

Received: October 28, 2024
Revised: February 23, 2025
Accepted: May 19, 2025
Published: June 13, 2025

REFERENCES

1. Squire, L.R. (1992). Memory and the hippocampus: a synthesis from findings with rats, monkeys, and humans. Psychol. Rev. *99*, 195–231. https://doi.org/10.1037/0033-295x.99.2.195.
2. Eichenbaum, H., and Cohen, N.J. (2001). From Conditioning to Conscious Recollection: Memory Systems of the Brain (Oxford University Press).
3. Morris, R.G.M., Amaral, D.G., Bliss, T.V., Duff, K.E.K., and O'Keefe, J. (2024). The Hippocampus Book, Second Edition (Oxford University Press).
4. O'Keefe, J., and Nadel, L. (1978). The Hippocampus as a Cognitive Map (Oxford University Press).
5. O'Keefe, J., and Dostrovsky, J. (1971). The hippocampus as a spatial map. Preliminary evidence from unit activity in the freely-moving rat. Brain Res. *34*, 171–175. https://doi.org/10.1016/0006-8993(71)90358-1.
6. Wilson, M.A., and McNaughton, B.L. (1993). Dynamics of the hippocampal ensemble code for space. Science *261*, 1055–1058. https://doi.org/10.1126/science.8351520.
7. Leutgeb, S., Leutgeb, J.K., Treves, A., Moser, M.-B., and Moser, E.I. (2004). Distinct ensemble codes in hippocampal areas CA3 and CA1. Science *305*, 1295–1298. https://doi.org/10.1126/science.1100265.
8. Harvey, C.D., Collman, F., Dombeck, D.A., and Tank, D.W. (2009). Intracellular dynamics of hippocampal place cells during virtual navigation. Nature *461*, 941–946. https://doi.org/10.1038/nature08499.
9. Ulanovsky, N., and Moss, C.F. (2007). Hippocampal cellular and network activity in freely moving echolocating bats. Nat. Neurosci. *10*, 224–233. https://doi.org/10.1038/nn1829.
10. Lee, A.K., and Wilson, M.A. (2002). Memory of sequential experience in the hippocampus during slow wave sleep. Neuron *36*, 1183–1194. https://doi.org/10.1016/s0896-6273(02)01096-6.
11. Foster, D.J., and Wilson, M.A. (2006). Reverse replay of behavioural sequences in hippocampal place cells during the awake state. Nature *440*, 680–683. https://doi.org/10.1038/nature04587.
12. Diba, K., and Buzsáki, G. (2007). Forward and reverse hippocampal place-cell sequences during ripples. Nat. Neurosci. *10*, 1241–1242. https://doi.org/10.1038/nn1961.
13. Gillespie, A.K., Astudillo Maya, D.A., Denovellis, E.L., Liu, D.F., Kastner, D. B., Coulter, M.E., Roumis, D.K., Eden, U.T., and Frank, L.M. (2021). Hippocampal replay reflects specific past experiences rather than a plan for subsequent choice. Neuron *109*, 3149–3163.e6. https://doi.org/10.1016/j.neuron.2021.07.029.
14. Carr, M.F., Jadhav, S.P., and Frank, L.M. (2011). Hippocampal replay in the awake state: a potential substrate for memory consolidation and retrieval. Nat. Neurosci. *14*, 147–153. https://doi.org/10.1038/nn.2732.
15. Foster, D.J. (2017). Replay comes of age. Annu. Rev. Neurosci. *40*, 581–602. https://doi.org/10.1146/annurev-neuro-072116-031538.
16. van der Meer, M.A.A., Kemere, C., and Diba, K. (2020). Progress and issues in second-order analysis of hippocampal replay. Philos. Trans. R. Soc. Lond. B Biol. Sci. *375*, 20190238. https://doi.org/10.1098/rstb.2019.0238.
17. Redish, A.D. (2020). Beyond replay: Introduction to the special issue on hippocampal replay. Hippocampus *30*, 3–5. https://doi.org/10.1002/hipo.23184.
18. Girardeau, G., Benchenane, K., Wiener, S.I., Buzsáki, G., and Zugaro, M. B. (2009). Selective suppression of hippocampal ripples impairs spatial memory. Nat. Neurosci. *12*, 1222–1223. https://doi.org/10.1038/nn.2384.
19. Ego-Stengel, V., and Wilson, M.A. (2010). Disruption of ripple-associated hippocampal activity during rest impairs spatial learning in the rat. Hippocampus *20*, 1–10. https://doi.org/10.1002/hipo.20707.
20. Jadhav, S.P., Kemere, C., German, P.W., and Frank, L.M. (2012). Awake hippocampal sharp-wave ripples support spatial memory. Science *336*, 1454–1458. https://doi.org/10.1126/science.1217230.
21. Gridchyn, I., Schoenenberger, P., O'Neill, J., and Csicsvari, J. (2020). Assembly-specific disruption of hippocampal replay leads to selective memory deficit. Neuron *106*, 291–300.e6. https://doi.org/10.1016/j.neuron.2020.01.021.
22. Buzsáki, G. (1989). Two-stage model of memory trace formation: a role for "noisy" brain states. Neuroscience *31*, 551–570. https://doi.org/10.1016/0306-4522(89)90423-5.
23. Buzsáki, G. (1996). The hippocampo-neocortical dialogue. Cereb. Cortex *6*, 81–92. https://doi.org/10.1093/cercor/6.2.81.
24. Battaglia, F.P., Sutherland, G.R., and McNaughton, B.L. (2004). Hippocampal sharp wave bursts coincide with neocortical "up-state" transitions. Learn. Mem. *11*, 697–704. https://doi.org/10.1101/lm.73504.
25. Wang, S.H., and Morris, R.G.M. (2010). Hippocampal-neocortical interactions in memory formation, consolidation, and reconsolidation. Annu. Rev. Psychol. *61*, 49–79. https://doi.org/10.1146/annurev.psych.093008.100523.
26. Pfeiffer, B.E., and Foster, D.J. (2013). Hippocampal place-cell sequences depict future paths to remembered goals. Nature *497*, 74–79. https://doi.org/10.1038/nature12112.
27. Pezzulo, G., van der Meer, M.A.A., Lansink, C.S., and Pennartz, C.M.A. (2014). Internally generated sequences in learning and executing goal-directed behavior. Trends Cogn. Sci. *18*, 647–657. https://doi.org/10.1016/j.tics.2014.06.011.
28. Davidson, T.J., Kloosterman, F., and Wilson, M.A. (2009). Hippocampal replay of extended experience. Neuron *63*, 497–507. https://doi.org/10.1016/j.neuron.2009.07.027.
29. Eliav, T., Maimon, S.R., Aljadeff, J., Tsodyks, M., Ginosar, G., Las, L., and Ulanovsky, N. (2021). Multiscale representation of very large environments in the hippocampus of flying bats. Science *372*, eabg4020. https://doi.org/10.1126/science.abg4020.
30. Denovellis, E.L., Gillespie, A.K., Coulter, M.E., Sosa, M., Chung, J.E., Eden, U.T., and Frank, L.M. (2021). Hippocampal replay of experience at real-world speeds. eLife *10*, e64505. https://doi.org/10.7554/eLife.64505.
31. McNaughton, B.L., Barnes, C.A., and O'Keefe, J. (1983). The contributions of position, direction, and velocity to single unit activity in the hippocampus of freely-moving rats. Exp. Brain Res. *52*, 41–49. https://doi.org/10.1007/BF00237147.
32. Karlsson, M.P., and Frank, L.M. (2009). Awake replay of remote experiences in the hippocampus. Nat. Neurosci. *12*, 913–918. https://doi.org/10.1038/nn.2344.
33. Ziv, Y., Burns, L.D., Cocker, E.D., Hamel, E.O., Ghosh, K.K., Kitch, L.J., El Gamal, A., and Schnitzer, M.J. (2013). Long-term dynamics of CA1 hippocampal place codes. Nat. Neurosci. *16*, 264–266. https://doi.org/10.1038/nn.3329.
34. Drieu, C., Todorova, R., and Zugaro, M. (2018). Nested sequences of hippocampal assemblies during behavior support subsequent sleep replay. Science *362*, 675–679. https://doi.org/10.1126/science.aat2952.
35. Sarel, A., Palgi, S., Blum, D., Aljadeff, J., Las, L., and Ulanovsky, N. (2022). Natural switches in behaviour rapidly modulate hippocampal coding. Nature *609*, 119–127. https://doi.org/10.1038/s41586-022-05112-2.
36. Tsoar, A., Nathan, R., Bartan, Y., Vyssotski, A., Dell'Omo, G., and Ulanovsky, N. (2011). Large-scale navigational map in a mammal. Proc. Natl. Acad. Sci. USA *108*, E718–E724. https://doi.org/10.1073/pnas.1107365108.
37. Gobet, F., Lane, P.C.R., Croker, S., Cheng, P.C.-H., Jones, G., Oliver, I., and Pine, J.M. (2001). Chunking mechanisms in human learning. Trends Cogn. Sci. *5*, 236–243. https://doi.org/10.1016/s1364-6613(00)01662-4.
38. Ben-Yakov, A., and Henson, R.N. (2018). The hippocampal film editor: sensitivity and specificity to event boundaries in continuous experience. J. Neurosci. *38*, 10057–10068. https://doi.org/10.1523/JNEUROSCI.0524-18.2018.
39. Zheng, J., Schjetnan, A.G.P., Yebra, M., Gomes, B.A., Mosher, C.P., Kalia, S.K., Valiante, T.A., Mamelak, A.N., Kreiman, G., and Rutishauser, U.

(2022). Neurons detect cognitive boundaries to structure episodic memories in humans. Nat. Neurosci. *25*, 358–368. https://doi.org/10.1038/s41593-022-01020-w.

40. Hahamy, A., Dubossarsky, H., and Behrens, T.E.J. (2023). The human brain reactivates context-specific past information at event boundaries of naturalistic experiences. Nat. Neurosci. *26*, 1080–1089. https://doi.org/10.1038/s41593-023-01331-6.

41. Roscow, E.L., Chua, R., Costa, R.P., Jones, M.W., and Lepora, N. (2021). Learning offline: memory replay in biological and artificial reinforcement learning. Trends Neurosci. *44*, 808–821. https://doi.org/10.1016/j.tins.2021.07.007.

42. Keskar, N.S., Nocedal, J., Tang, P.T.P., Mudigere, D., and Smelyanskiy, M. (2017). On large-batch training for deep learning: generalization gap and sharp minima. ICLR International Conference on Learning Representations 5.

43. Banerjee, S., and Chakraborty, S. (2021). Deterministic mini-batch sequencing for training deep neural networks. AAAI *35*, 6723–6731. https://doi.org/10.1609/aaai.v35i8.16831.

44. Hafner, D., Lillicrap, T.P., Norouzi, M., and Ba, J. (2021). Mastering Atari with discrete world models. ICLR International Conference on Learning Representations 9.

45. Danilovich, S., Krishnan, A., Lee, W.-J., Borrisov, I., Eitan, O., Kosa, G., Moss, C.F., and Yovel, Y. (2015). Bats regulate biosonar based on the availability of visual information. Curr. Biol. *25*, R1124–R1125. https://doi.org/10.1016/j.cub.2015.11.003.

46. Geva-Sagiv, M., Las, L., Yovel, Y., and Ulanovsky, N. (2015). Spatial cognition in bats and rats: from sensory acquisition to multiscale maps and navigation. Nat. Rev. Neurosci. *16*, 94–108. https://doi.org/10.1038/nrn3888.

47. Joshi, A., Denovellis, E.L., Mankili, A., Meneksedag, Y., Davidson, T.J., Gillespie, A.K., Guidera, J.A., Roumis, D., and Frank, L.M. (2023). Dynamic synchronization between hippocampal representations and stepping. Nature *617*, 125–131. https://doi.org/10.1038/s41586-023-05928-6.

48. Kloosterman, F., Layton, S.P., Chen, Z., and Wilson, M.A. (2014). Bayesian decoding using unsorted spikes in the rat hippocampus. J. Neurophysiol. *111*, 217–227. https://doi.org/10.1152/jn.01046.2012.

49. Toft, P. (1996). The radon transform – theory and Implementation. PhD thesis (Technical University of Denmark).

50. Tingley, D., and Peyrache, A. (2020). On the methods for reactivation and replay analysis. Philos. Trans. R. Soc. Lond. B Biol. Sci. *375*, 20190231. https://doi.org/10.1098/rstb.2019.0231.

51. Kay, K., Sosa, M., Chung, J.E., Karlsson, M.P., Larkin, M.C., and Frank, L.M. (2016). A hippocampal network for spatial coding during immobility and sleep. Nature *531*, 185–190. https://doi.org/10.1038/nature17144.

STAR★METHODS

KEY RESOURCES TABLE

REAGENT or RESOURCE	SOURCE	IDENTIFIER
Deposited data		
Raw and analyzed data, including electrophysiological and behavioral data	This paper	Available upon request
Experimental models: Organisms/strains		
Egyptian fruit bats (*Rousettus aegyptiacus*)	Wild-born bats caught in Israel or bred in captivity	N/A
Software and algorithms		
MATLAB R2021b	MathWorks	https://www.mathworks.com/products/matlab.html
Offline Sorter (spike-sorting software)	Plexon	https://plexon.com/products/offline-sorter/
Replay trajectory classification (python package for clusterless decoding)	Denovellis et al.[30]	https://github.com/Eden-Kramer-Lab/replay_trajectory_classification
Custom analysis code	This paper	Original code used in this study is publicly available at Zenodo, at https://doi.org/10.5281/zenodo.15330798.
Other		
Small animal stereotax	David Kopf Instruments	http://kopfinstruments.com/product/model-942-small-animal-stereotaxic-instrument-with-digital-display-console
Tetrode wire Platinum 90% Iridium 10% HML-insulated	California Fine Wire	https://calfinewire.com/
4-tetrode Microdrive	Neuralynx	https://neuralynx.fh-co.com/research-hardware/animal-interfaces/microdrives/harlan-4-drive/
16-tetrode microdrive	Custom made	N/A
Spikelog-16 or spikelog-64 (wireless neural logger)	Deuteron Technologies	https://deuterontech.com/
Ultra-wideband (UWB) radio-frequency-based localization system	BeSpoon – ST	https://www.st.com/en/wireless-connectivity/ultra-wideband-products.html

EXPERIMENTAL MODEL AND STUDY PARTICIPANT DETAILS

Animals, behavior, and electrophysiological recordings

All experimental procedures are reported in detail in Eliav et al.[29] (for the one-bat experiments: Figures 1, 2, and 3) and in Sarel et al.[35] (for the two-bat experiments: Figures 5C–5G); the 15-meter tunnel data (Figure 4) are from new experiments. In this study we analyzed data from sleep sessions and awake-pauses (see below); these data were not analyzed before. The experimental procedures were approved by the Institutional Animal Care and Use Committee of the Weizmann Institute of Science.

Nine adult male Egyptian fruit bats (*Rousettus aegyptiacus*), were included in this study as subjects for electrophysiological recordings. Seven bats were tested in single-bat flight experiments in the long tunnel[29] (Figures 1, 2, and 3, see below). Five of the seven bats were wild-born bats and two were lab-born bats; we included together the data from all seven bats because we previously showed that the coding properties of CA1 neurons in the long tunnel were very similar between wild-born and lab-born bats.[29] One additional wild-born bat (bat no. 8) was recorded in a shorter 15-m version of the tunnel (Figure 4) – as well as in a more complicated task in a long 180-m tunnel, involving a choice in a T-junction at its end, as well as back-and-forth shuttling (see details in Figure S5). An additional wild-born bat (bat no. 9) was recorded in two-bat flight experiments[35] (Figures 5C–5G). All experiments were conducted at relatively low light levels (5 lux), at which these highly-visual bats can see very well.[45,46] In all experiments, a human experimenter was sitting near the entrance-door to the tunnel, and in some of the sessions a second experimenter was sitting at the far end of the tunnel: both humans were outside of the area where the bats were flying.

We conducted neuronal recordings of single neurons in the dorsal hippocampus of these bats, using a wireless electrophysiology system, while the bats were flying back-and-forth in a very large environment — a long flight-tunnel (5 bats were recorded in a 200-meter long tunnel, 2 bats were recorded in a 130-meter portion of the tunnel, one bat was recorded in a 180-m portion of the tunnel, and the two-bat experiment was conducted in a 135-meter portion of the tunnel). To this end, the bats were implanted with a 4-tetrode or 16-tetrode microdrive. The microdrive was implanted above the right dorsal hippocampus, as described previously,[29,35] and then the tetrodes were slowly lowered towards the hippocampal CA1 pyramidal cell layer over a time period of 2–3 weeks, and recordings were subsequently collected from dorsal CA1. In one of the 9 bats we further lowered a few tetrodes to the CA3 pyramidal layer, and these were included in the analysis. Positioning of tetrodes in the CA1 pyramidal layer was provisionally assessed by the presence of high frequency field oscillations ('ripples') and associated neuronal firing, and in CA3 it was based on population bursting and nominal depth. Recording positions were later verified histologically. Neural recordings were conducted using a wireless neural-recording device (neural-logger; Deuteron Technologies) that filtered the neural signal between 1 – 7,000 Hz and then continuously sampled the signal at either 29.3 kHz or 31.25 kHz, and stored all the raw neuronal data on-board. The 3D position of the bat in the tunnel was tracked at a rate of 18.3 Hz or 14.2 Hz (for the 1-bat experiments) or 12.8 Hz (for the 2-bat experiment), using an ultra-wideband radio-frequency based localization system (BeSpoon – ST), with a precision of 9 cm in the horizontal plane.[29] The 3D position was projected onto the main axis of the tunnel, and only this 1D position was further analyzed here. The bats were flying between two landing-platforms located at the two ends of the tunnel, where they received food reward and could pause to rest between flight epochs (Figure 1A). These rest-pauses between flights were analyzed as described below, in search of awake replays. Each experimental day started with a sleep session and ended with a sleep session (each sleep session lasted typically ~10 minutes). For the sleep sessions, the bat was placed alone inside a small covered cage which was positioned in a quiet location inside the tunnel (not far from the entrance-door). These sleep sessions were analyzed as described below, in search of sleep replays.

METHOD DETAILS

Detecting multiunit spikes, and spike sorting of individual neurons

Continuous neural recordings from all channels were first high-pass filtered at 600 Hz, yielding neural signals that were band-limited between 600 – 7,000 Hz. A threshold was applied to detect spikes, set as: $threshold = 6 \times V_{noise}$, where the noise term was defined separately for each recording-channel as the median of the absolute values of the filtered signal across the entire recording session. Spikes were detected if any of the 4 channels in a given tetrode crossed the threshold. Then, 1-ms spike waveforms were extracted on all 4 channels simultaneously, and 4 features were defined for each spike as the amplitudes of the spike on each of the 4 channels of the tetrode. To eliminate noise, we compared the detected spike waveforms to a library of waveforms from 286 well-isolated bat hippocampal neurons previously recorded in the lab, and we excluded all spikes that had a correlation below 0.80 with all the waveforms in the library. Additionally, we also excluded all detected spikes that occurred simultaneously within < 0.15 ms across multiple tetrodes (across more than half of the tetrodes in the 16-tetrode microdrive, or across all the 4 tetrodes in the 4-tetrode microdrive) – including tetrodes that were not in the cell layer – which indicates a common noise.

Activity from all unsorted multiunit spikes was then used for decoding purposes, as well as for computing multiunit firing rates (see below).

In addition, for one of the figures (Figure 2), we also analyzed the activity of well-separated individual neurons, namely single-unit data. The spike sorting was done as described previously.[29,35] Briefly, spike waveforms were sorted manually using Plexon Offline Sorter, on the basis of their relative amplitudes on different channels of each tetrode. Data from all sessions – the behavioral session and the two sleep sessions – were spike-sorted together. Well-isolated clusters of spikes were manually selected, and a refractory period (< 2 ms) in the inter-spike-interval histogram was verified. We included in Figure 2 only neurons that were stably isolated throughout the recording.

Clusterless state-space decoder

To reconstruct position from neural activity, we employed a clusterless state-space decoding method, which was used in a number of previous studies in rodents.[13,30,47] For a detailed description of the method, see Denovellis et al.[30] In brief, the method consists of two main parts: (1) A clusterless maximum-likelihood decoder, which maps the feature space of spikes (the 4 amplitudes of each spike on the 4 channels of the tetrode, without any spike-sorting) to position along the tunnel; and (2) A state-space model which characterizes the dynamics in the spatial representations as a mixture of three underlying movement patterns: a stationary spatial representation, spatially continuous movement trajectories, and spatially discontinuous representation (see more below).

The combination of these two aspects of the decoding-method brings several advantages: (1) The clusterless decoder does not require any spike-sorting – a process that is usually done manually, and is thus both (i) laborious and (ii) subjective; both of these limitations are avoided by using clusterless decoding ('clusterless' means without clustering [spike-sorting] of spikes into distinct units [neurons]). (iii) The clusterless approach provides much more information for decoding, as compared to spike-sorted data, because it utilizes the many spikes which cannot be sorted into well-isolated clusters but which nevertheless carry useful information about the animal's behavior (the bat's position). Consequently, a clusterless decoding approach yields a much superior decoding accuracy.[30,48] (2) The state-space model provides direct information that the decoded position is moving through space (see also the section 'detecting replay events during sleep and awake', below). (3) This method enables decoding position from neural activity

at very high temporal resolution (millisecond-scale).[13,30,47] This high temporal resolution is important for being able to detect highly compressed replays that depict long-distance trajectories within a short time-duration.

Encoding

To train the model we provided it with the neural activity (unsorted spike features [amplitudes], see above), together with the animal's position along the tunnel, and its flight direction. The position along the tunnel was binned in 1-m bins (or 0.5-m bins for the data in the 15-m short tunnel, Figure 4). Encoding (training) data included only times during flight, where flight was defined as epochs which consisted of direct continuous trajectories that proceeded in the same direction over at least 100 meters (or 5 meters for the data from the 15-m short tunnel, Figure 4). We applied a speed threshold of 1 m/s, which included all the flight (the averaged flight speed was ~7–8 m/s) as well as the takeoff and landing parts of the flight epochs – while strictly excluding any stationary times. The model encoded the data by relating the spike features (spike amplitudes in the 4 channels of each tetrode) to the bat's position in the tunnel, using the joint probability distribution of spike features and bat-position (using a kernel density estimation of this joint distribution) – as done in Denovellis et al.[30] – although we used here different Gaussian kernel widths that were more suitable for our data and empirically provided better accuracy of decoding during behavior: Gaussian kernels with SD of 2 meters for the position dimension, and SD of 20 μV for the spike amplitude feature dimensions. Importantly, the two movement directions in the tunnel, which we showed to have different spatial representations,[29] were encoded separately in the model.

Decoding

We decoded separately during (i) flight epochs, (ii) sleep sessions when the bat was in the cage, and (iii) awake pause epochs on the platforms, between flights. To decode the bat's position from the neural activity, we first binned the neural activity into 2-ms time-bins – the same time-bin that was used in previous studies of replay in rodents that employed this decoding method.[13,30] Then, we used the kernel density estimation to obtain the position likelihood given the spikes' amplitudes. Next, we utilized the state-space model (see below) to estimate simultaneously the posterior probabilities of both the position and the movement dynamics (the model had 3 types of dynamics for each of the 2 maps [the maps for the 2 directions]: stationary, continuous movement, or discontinuous movement – i.e. 6 states in total [3 dynamics $\times$ 2 maps = 6 states]). We applied a forward-backwards algorithm: a causal (forward) filter followed by an acausal smoother (backwards). This was done using the state transitions matrix and movements dynamics matrices of the state-space model – see Denovellis et al.[30] (we set a probability of 0.98 to persist in the same state in two consecutive time-bins of 2-ms, and a probability of 0.02 to switch states – this is the same probability-value as used in previous studies of replay in rodents that employed this decoding method[13,30]). This information, which was integrated from both past and future neural activity, was used in order to estimate the position and movement dynamics in any given time-bin, at 2-ms temporal resolution (2-ms bins) and 1-meter spatial resolution (1-m bins). In total, the model provided an estimation of the joint posterior probability of position and movement dynamics at each time bin k: $\Pr(X_k, I_k | O_{1:T})$, where X is the position in the tunnel (in 1-meter bins), and I is a set of 6 states (3 movement dynamics [stationary, continuous movement, and discontinuous] $\times$ 2 movement directions). This joint posterior probability distribution was evaluated at every time bin k (with $1 \leq k \leq T$, where T is the number of time-bins in the decoded epoch, i.e. in the sleep session or in an individual awake-pause epoch) – given the observed neural activity at times $1:T$, denoted as $O_{1:T}$.

Probability of movement dynamics

The decoded probability of each movement dynamics indicates the contribution of each of the states to the total joint posterior probability, and is computed by integrating the probability over all positions:

$$\Pr(I_k | O_{1:T}) = \sum_{X_k} \Pr(X_k, I_k | O_{1:T})$$

Probability of position

The decoded probability of position indicates the posterior probability function of position given all movement states, and is computed by integrating the probability over all states:

$$\Pr(X_k | O_{1:T}) = \sum_{I_k} \Pr(X_k, I_k | O_{1:T})$$

The decoded position was taken as the position where this posterior probability function was maximal (maximum a-posteriori probability estimate).

The Python code package used for decoding was taken from Denovellis et al.,[30] and can be found here: https://github.com/Eden-Kramer-Lab/replay_trajectory_classification.

Quantifying decoding-accuracy, and inclusion criteria for sessions

We quantified the decoding accuracy by comparing the decoded position to the ground-truth position during actual flight. To this end, we used a leave-one-out approach, where for each flight epoch we trained the decoder using times from all the other flight epochs (train data), and then decoded the position during the one flight epoch which we excluded from training (test data). Each behavioral session (recording day) was analyzed separately. We subsequently only included data from sessions that exhibited high decoding quality during *flight* (during behavior) – and then we looked for replays in the *same* high-quality sessions during sleep and during awake-pauses. The criteria for high-quality decoding during flight were as follows: (i) The median position estimation error was < 2% of the environment size (or < 5% for the 15-m environment). (ii) Decoding accuracy during behavior (in-flight) was ≥70%,

whereby we considered position estimations as correct if they differed from the real position of the bat by less than 5% of the environment size; in other words, we required that ≥70% of the 2-ms time bins during flight were decoded with high spatial accuracy of 5% as compared to the ground-truth. In total, 82 sessions from 7 bats passed these criteria and were included for further analysis. These data included both experiments where the bat flew over the entire 200-meter tunnel (5 bats, 39 sessions), and experiments where the bat flew over a 130-meter portion of the tunnel (2 bats, 43 sessions). We also included data from 5 sessions from the two-bat experiment (1 recorded bat), which passed these criteria; this bat was flying in a 135-meter portion of the tunnel and was crossing-over another bat.[35] Finally, we included also data from 6 sessions in the 15-meter small environment.

Detecting replay events during sleep and awake

The state-space model provides the decoded posterior probability of both position and movement dynamics. Therefore, we could use the movement-dynamics probability to detect events of coherent continuous movement trajectories – i.e., sequential replay events. We detected such replay events by setting a probability-threshold of $p > 0.8$ for the continuous movement dynamics (separately for each movement direction). To allow detecting longer-duration and longer-distance replays that may have went below the $p = 0.8$ threshold for a brief moment (for less than 100 ms), we merged together any crossings of this threshold that were < 100 ms apart (this merging occurred in 0.39% of the replay events [28 out of 7,213]). The start and end times of each replay event were set as the times that the probability of the continuous movement dynamics state dropped below $p = 0.5$: these were used to define the *replay duration*. We then applied additional criteria on replays, as detailed in the next section.

We note that the replays were decoded irrespective of the occurrence of sharp-wave ripples in the LFP, and irrespective of the multiunit firing-rate – but we later verified that the decoded replays usually co-occurred with sharp-wave ripples and with increased multiunit firing-rate (Figures 1H and 1I) – as shown previously in rodents.[28,30]

This approach for detecting replays has two important advantages: First, it uses a state-space model that captures the movement dynamics probability, in addition to the position – which gives a statistical framework that provides an estimation of trajectories that are represented in the neural activity. This statistical framework is interpretable, as it directly yields the probability that the hippocampal population activity represents each of the 6 states at every moment – and in particular, the probability that the bat (or the replay) is moving through space. Second, it provides an unbiased method to detect replays, unlike the classical methods that typically analyze only the activity during sharp-wave ripples or during high momentary population firing-rate. Moreover, these classical methods use a somewhat arbitrary definition for replay start and end times, based on ripple-band magnitude or multiunit activity firing-rate, which can potentially result in identifying only part of the real replay sequence. Instead, here we used the movement dynamics probability from the state-space model, which provides more direct information about the precise boundaries (start and end) of the actual replay event.

Quantifying replays, and inclusion criteria for replays

To quantify replay events, we employed the Radon transform, using an approach similar to Davidson et al.[28] and Denovellis et al.[30] This was done as follows: for each replay event we extracted the probabilities to be in each position given the movement dynamics of that replay event. This yielded a probability matrix of *n* rows (position bins) and *m* columns (time bins): see examples for such matrices in Figures 1F and 1G (bottom). We then convolved this matrix in the position-dimension using a rectangular window of ±5 m (such that each positional bin contained the sum of probabilities within a 5-m distance [for the 15-m experiment we used a ±1.5-m window]), and then densely sampled lines along this matrix and summed the probabilities along each line – a procedure known as the Radon transform,[49] which is widely used in image-analysis to detect lines in an image, and was used previously in a number of hippocampal studied to quantify replays.[28,30,50] We then selected the line with the maximal summed probabilities (see examples in Figures 1F and 1G, red lines). Then, we computed the *replay score*, which is a standard score used to quantify hippocampal replay,[28,30,50] and is defined as the mean probability along this best-fitted line; since the replay score is a probability value, it is bounded between 0 and 1. In other words: this procedure detected replay events in which the decoded position versus time was relatively linear – akin to the linear progression of the bat's position over time during actual behavior (due to its highly-stable flight speed[29]). [The convolution with a spatial rectangular window of ±5 m was done only for computing the Radon transform and replay score, and was not applied when displaying the matrices (e.g. in Figures 1F and 1G); this ±5 m convolution was done in order to allow quantifying position-versus-time for replay trajectories that are not perfectly linear, but are slightly deviating from a straight line, by up to ±5 m.] Using the line fitted by the Radon transform, we defined several quantities: (i) the positions of the start and end of the replay event, which allow extracting the *replay distance*; (ii) the *replay speed*, defined as the slope of this best-fitted line; (iii) the *compression-ratio* of the replay event, which was defined as the replay speed divided by the median speed during real flights in that behavioral session. We also defined (iv) the *replay position*, as the mid-point of the linear fit to the replay (e.g., the middle of the red lines in Figures 1Fand 1G): this definition was used for *all* the analyses involving the positions of replays in the tunnel (unless indicated otherwise).

We further included for analysis only replay events that met the following criteria:

(i) Replay score > 0.5 – this criterion ensured a high-probability nearly-linear replay. (ii) Replay duration > 50 ms. (iii) Replay distance > 3 bins – this criterion ensured that the replay progressed a minimal distance, and was not static (this corresponds to 3-m in the long tunnel, where we used 1-m bins, and to 1.5-m in the 15-m short tunnel, where we used 0.5-m bins). The decoder parameters and the selection criteria for replays were *identical* for all our datasets – namely, when decoding the data from the long tunnel, the 15-m short tunnel, and the two-bat experiment. For analyzing the replay-position during the two-bat experiments versus the

cross-over positions between the bats (Figures 5F and 5G), we required another inclusion-criterion: that the replay-center occurred > 8 meters from a landing-platform; this criterion was used only for this particular analysis, because the cross-over positions were computed only for locations > 8 meters from the landing-platforms.[35]

Note that for replay quantification we did not sum probabilities over all the 6 possible movement-dynamics states – but rather focused only on the current movement state. This was done in order to avoid erroneous line fitting that is biased by probabilities in different positions coming from different states. For display purposes we used the position probability of the current state (Figures 1F, 1G, 4C, 5E, S1, S2, and S5).

Computing firing-rates maps for individual neurons, in-flight and within-replays

Individual neurons were spike-sorted as described in Eliav et al.[29] We then constructed two types of firing-rate maps, for well-isolated individual neurons (see Figures 2A and 2D).

In-flight firing-rate maps

These standard firing-rate maps were constructed using only flight periods, separately for the two flight directions, as described in Eliav et al.[29] In brief, individual flights were identified based on local peaks in the flight speed that had maximal-speed > 4 m/s without changes in flight direction. The beginning and end of each flight was taken as the time-point where the bat's speed crossed a threshold of 1 m/s. We included in further analysis only unidirectional flight-trajectories longer than 100 meters, and the spikes that occurred during these flight-trajectories; only sessions with more than 10 such long flights per direction were included for further analysis. To compute the standard 1D firing-rate maps in-flight, we used fixed-sized spatial bins (20 cm) and collapsed the time-spent (occupancy) data and the spike counts onto the horizontal 1D dimension along the tunnel (linearized position). We smoothed both the spike-count and time-spent 1D maps with a Gaussian kernel (σ = 2.5 bins = 0.5 m), and then divided, bin by bin, the smoothed 1D spike-count by the smoothed 1D time spent – to produce the firing-rate map (Figure 2D, black curves). Place fields (whose peak-locations were used in Figures 2B and 2C, middle column) were detected as in Eliav et al.[29]

Within-replay firing-rate maps

These non-standard firing-rate maps were constructed similarly to the standard in-flight firing-rate maps – using the same binning (20 cm) and same smoothing (σ = 2.5 bins = 0.5 m) – but instead of using the actual position in-flight, we used here the *decoded* position during replays. Specifically, we counted the spikes in each decoded position during replays, and then normalized them by the time spent in that decoded position during replays – pooling all the replays in that session (both awake replays and sleep replays) – thus producing a firing-rate map within-replay (examples: Figure 2D, red curves).

Sharp-wave ripples, and multiunit activity

Sharp-wave ripples were detected using methods similar to Ulanovsky and Moss,[9] Lee and Wilson,[10] Gillespie et al.,[13] Denovellis et al.,[30] and Kay et al.[51] First, local field potentials from all tetrodes in CA1 (but not CA3) were obtained by filtering the continuous neural activity between 1 Hz and 400 Hz, and downsampling it from the original ~30 kHz sample-rate to 2 kHz. Then, a bandpass filter in the ripple band (100–200 Hz) was applied, and the square of the absolute of the Hilbert transform was summed across all tetrodes and was further smoothed with a Gaussian kernel of 4 ms. The square root of this trace was taken as the population ripple-band power. We then *z*-scored this power using the mean and SD calculated only from the sleep sessions or awake-pause periods (separately for sleep and awake). Candidate sharp-wave ripple events were detected as times when the z-scored power crossed 2.5 SD; events separated in time by less than 25 ms were merged; we excluded events shorter than 25 ms.

Multiunit activity was calculated by binning the unsorted multiunit spikes from each tetrode in 1-ms bins, and smoothing the firing-rate with a Gaussian kernel with σ = 15 ms. A *z*-scored firing-rate was then calculated using the mean and SD from the sleep sessions or awake-pause periods (separately for sleep and awake).

Data and code availability

Data reported in this paper are available from the lead contact upon request. Any additional information required to reanalyze the data reported in this work is available from the lead contact upon request. All the behavioral and neural data in this study were analyzed using custom code written in Matlab, and the state-space decoder analysis was performed in Python. The Python code package used for decoding was taken from Denovellis et al.,[30] and can be found here: https://github.com/Eden-Kramer-Lab/replay_trajectory_classification. Original code used in this study has been deposited at Zenodo and is publicly available at https://doi.org/10.5281/zenodo.15330798 as of the date of publication.

QUANTIFICATION AND STATISTICAL ANALYSIS

Details of statistical tests can be found in the figure legends. Unless otherwise specified, measured values and ranges represent mean ± SEM. Significance was defined as $p < 0.05$. Sample sizes were not predetermined by statistical methods, but efforts were made to collect as many samples as was technically feasible. See 'method details' for inclusion criteria for sessions and replays; no data or subjects were further excluded from any analysis.

Supplemental figures

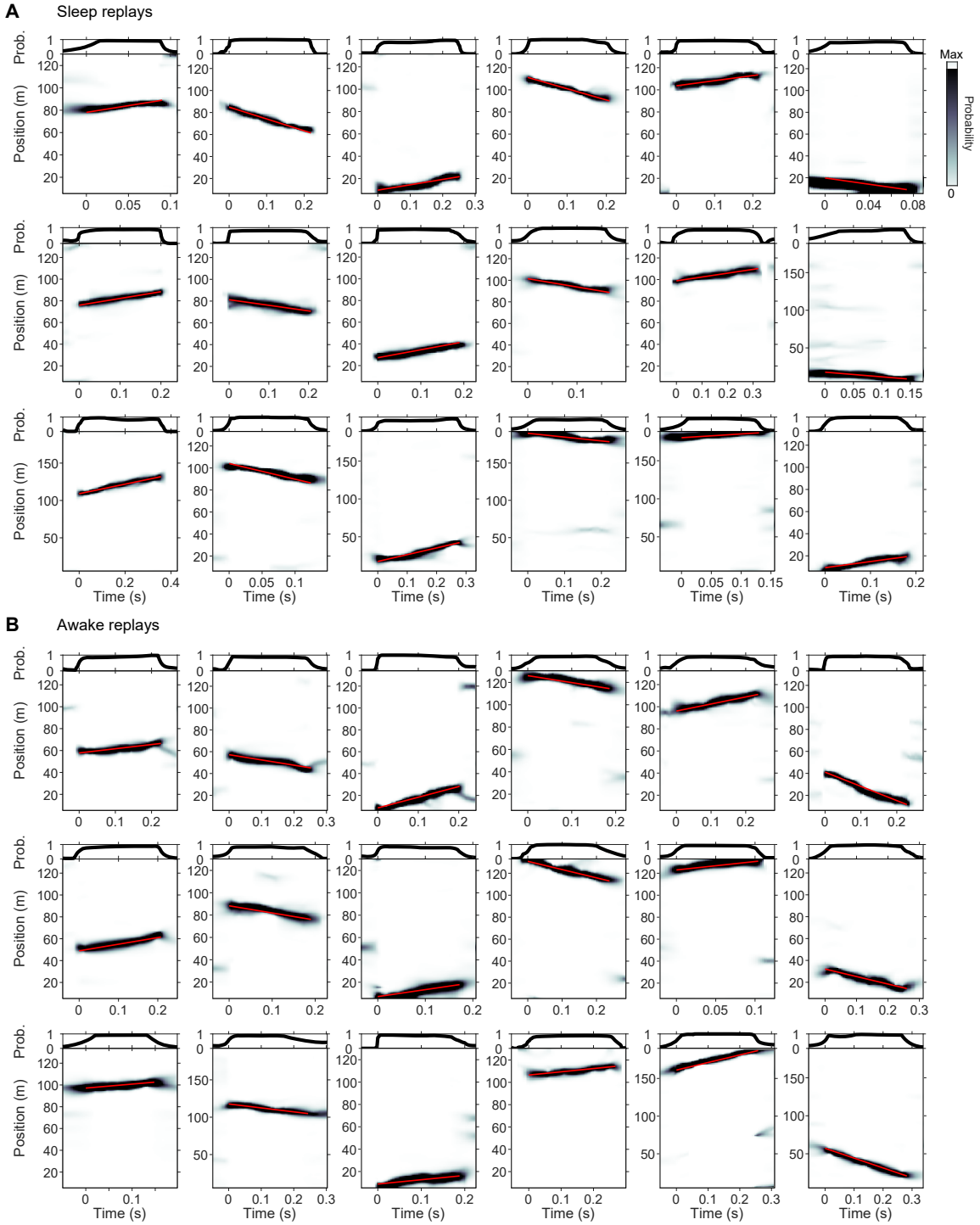

Figure S1. Additional examples of sleep-replay and awake-replay events, related to Figure 1

(A and B) Additional examples of replays from sleep (A) and awake (B), plotted as in main Figures 1F and 1G.

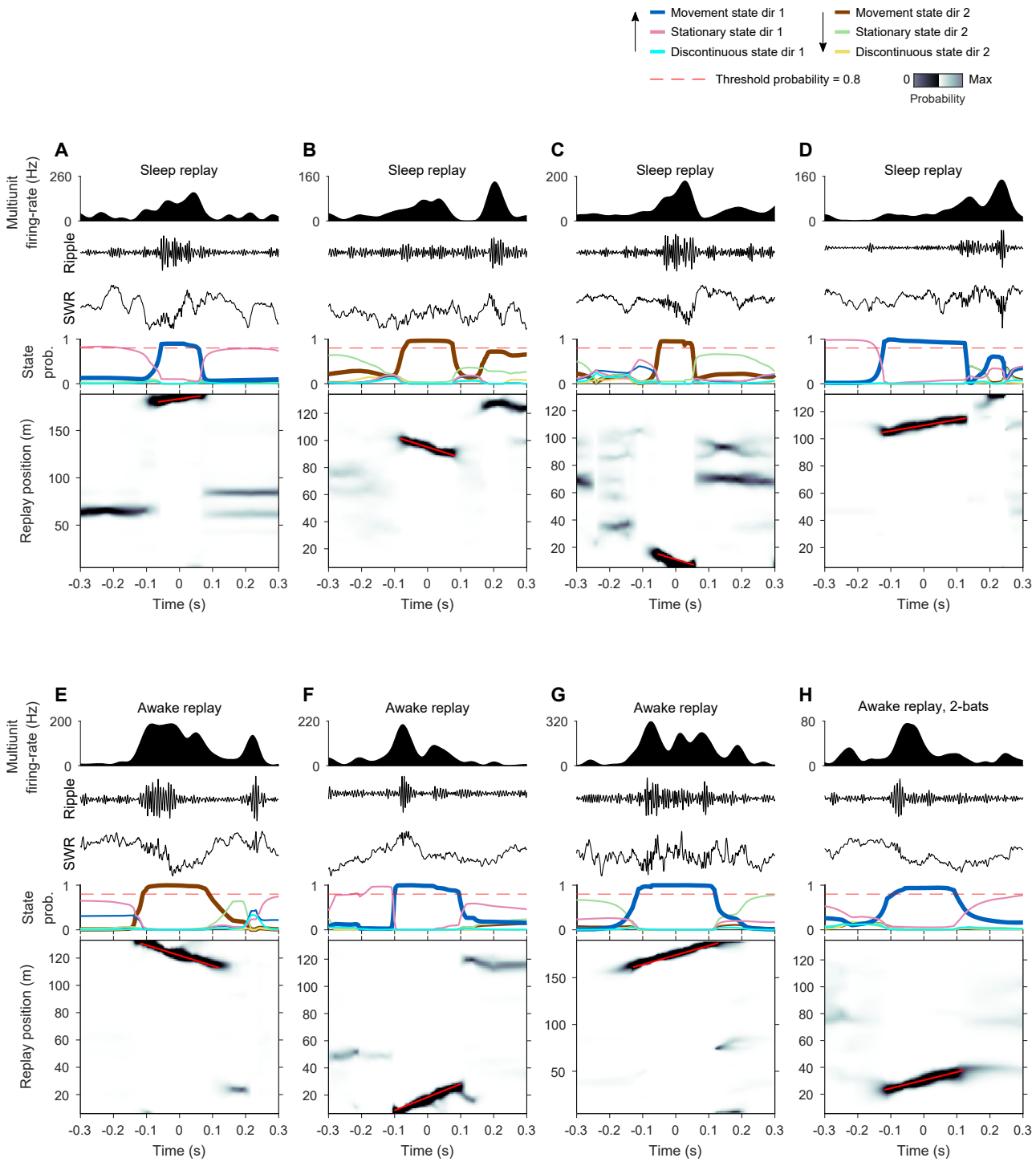

Figure S2. Full examples of eight replay events, including multiunit activity, ripple local field potential, and all the six states of the state-space decoder, related to Figure 1

(A–H) Examples of eight replay events, plotted here in more detail: four examples of sleep replays, three awake replays, and one awake replay from the two-bat experiment (these include two examples from main Figure 1F, the one example from main Figure 5E, and five examples from Figure S1). For each example, the five panels show (from top to bottom): panel 1: multiunit activity firing rate, averaged over all the tetrodes that were located during that session in the pyramidal cell layer of the hippocampus (these tetrodes were used for decoding this replay event). Note the clear increase in population firing rate that accompanied the replay

(legend continued on next page)

events. Panel 2 (ripple): local field potential from one of the tetrodes in the hippocampus, filtered at ripple frequencies (100–200 Hz). Note the clear ripples that accompanied the replay events. Panel 3 ("SWR"): same sharp-wave ripple (SWR) as above, filtered at a broader frequency range (1–400 Hz). Many of the high-frequency ripples occurred on top of slower sharp-waves. Panel 4 ("state prob."): posterior probability of each of the 6 states of the state-space decoder—movement state/stationary state/discontinuous state for the two movement directions (see color legend, which also includes the map direction [black arrows]). Note the clear increase in the probability of the movement state, which crossed the threshold of probability $p = 0.8$ (red dashed horizontal line)—indicating a replay event. Panel 5: decoded positions (posterior probability) versus time, plotted only for the detected movement state; red line shows the duration and slope of the replay (fitted using the Radon transform). Time 0 here is the replay center (mid-point of the detected replay).

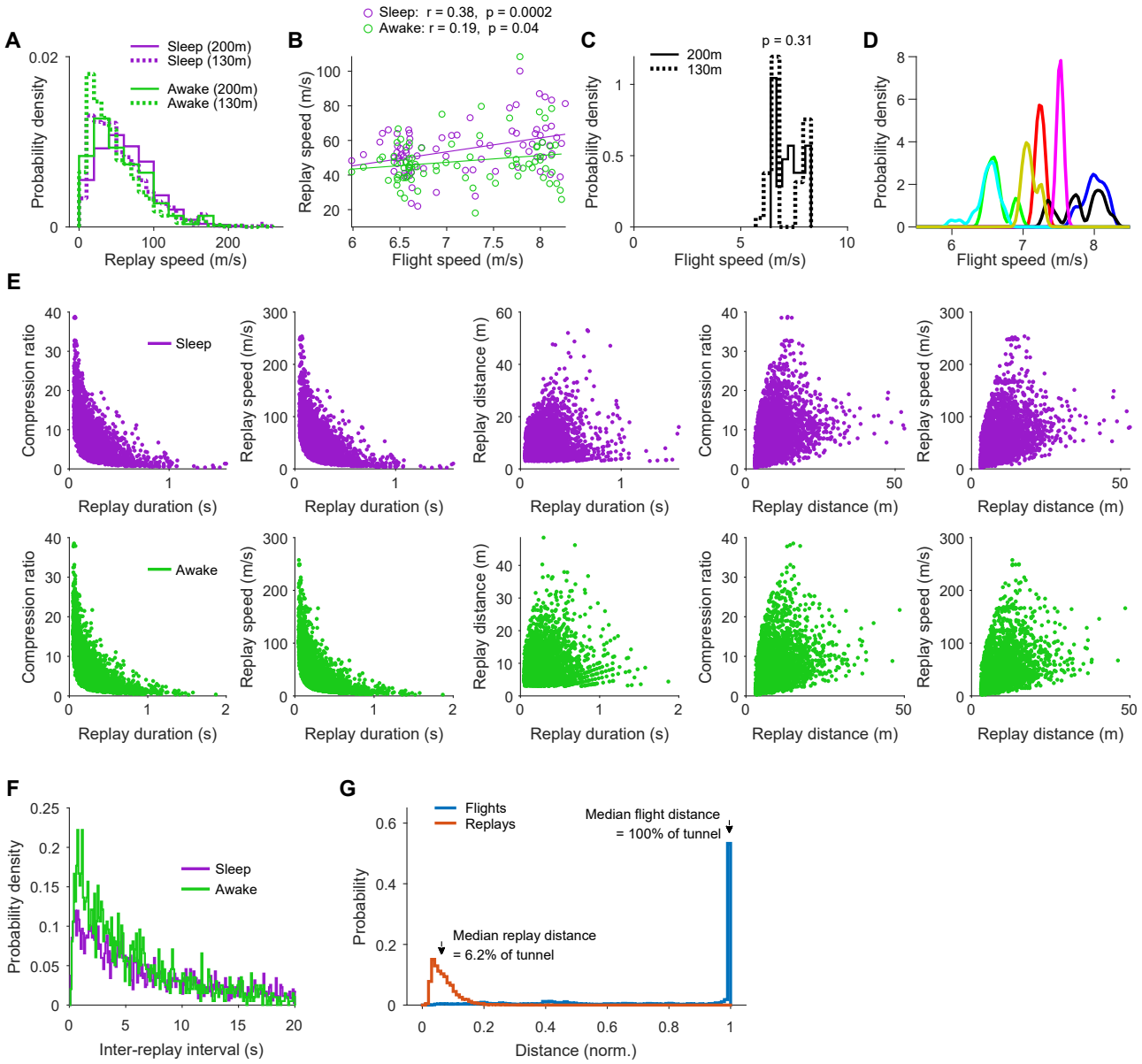

Figure S3. Replay speed and flight speed, and correlations of various replay parameters, related to Figure 3

(A) Distribution of replay speeds (m/s) for all the replays from all bats (n = 7,213 replays), plotted separately for replays during sleep (purple) and awake (green), for the 200-m tunnel (solid lines) and 130-m tunnel (dotted lines).

(B) Scatterplot of mean replay speed per session versus the median flight speed in that session, plotted separately for replays detected during sleep (purple) and during awake (green). Pearson correlations between replay speed and flight speed are indicated separately for sleep and awake (n = 82 sessions). We note that most of the variability in flight speed was due to individual differences between bats (see D), and therefore the correlation seen here implies that faster bats have faster replays.

(C) Distribution of median flight speed in each session for the 200-m tunnel (solid line, n = 39 sessions from 5 bats) and for the 130-m tunnel (dotted line, n = 43 sessions from 2 bats). Note that there was no significant difference in flight speeds between the 200-m tunnel and 130-m tunnel (t test, p = 0.31).

(D) Distributions of flight speeds for all the 7 individual bats that were analyzed in Figures 1, 2, and 3 (colors indicate individual bats; same colors as in Figure 1B; we plotted here the distribution of speeds across sessions, where for each session we computed the median flight speed in the session).

(E) Scatters of various replay parameters for all the sleep replays (top, purple) and awake replays (bottom, green) in the 7 bats that were analyzed in main Figures 1, 2, and 3.

(F) Distributions of inter-replay intervals during sleep (purple) and awake pauses (green).

(G) Distributions of replay distances (red) and flight distances (blue), normalized by the tunnel length (pooling together data from the 200- and 130-m-long tunnels, both sleep and awake replays). Note that while the bats exhibited continuous direct flights from one end of the tunnel to the other end (median of the blue distribution = 100% of the tunnel length, see right arrow), the replays were highly fragmented (median of the red distribution = 6.2% of the tunnel length, see left arrow).

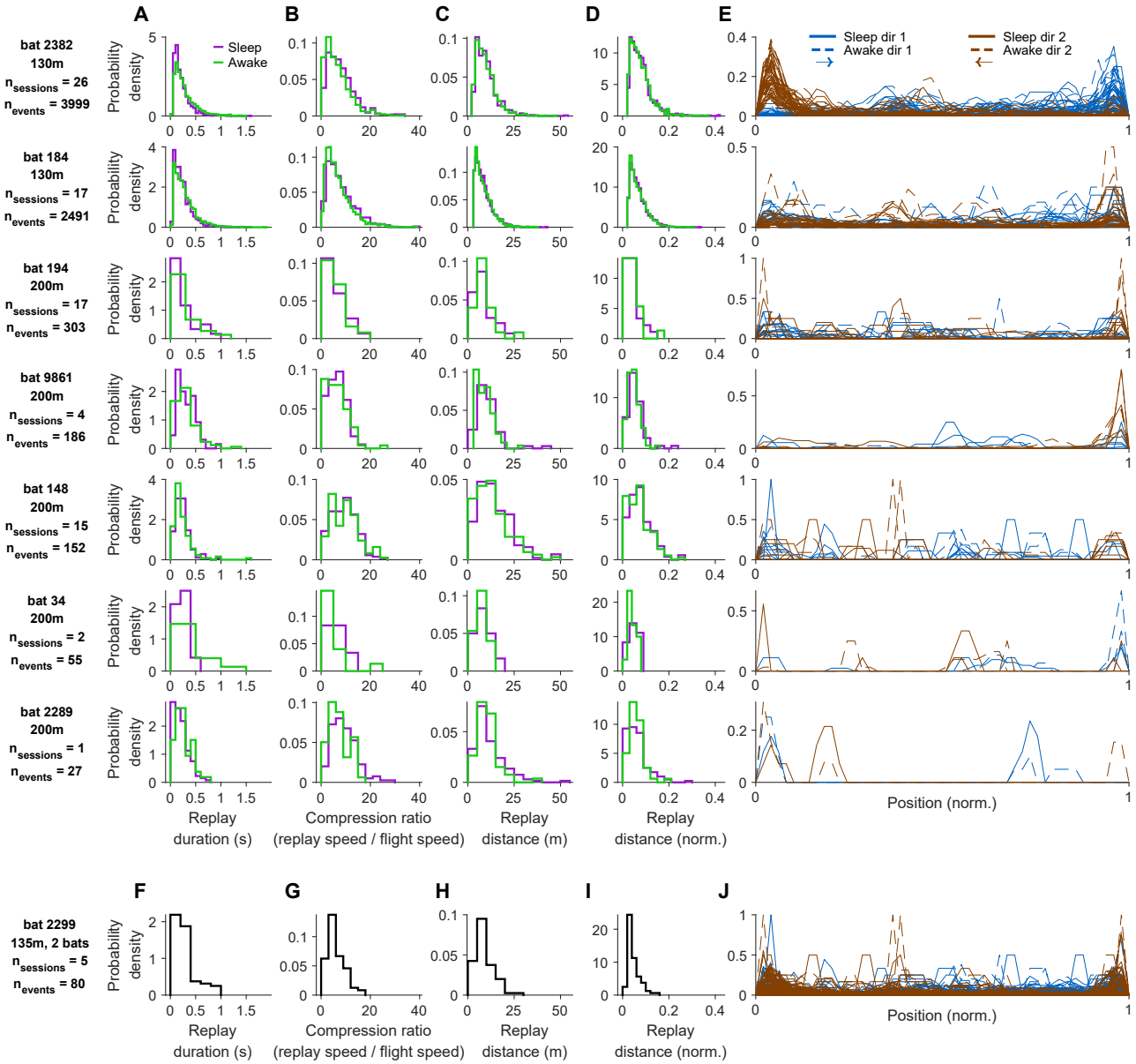

Figure S4. Population summaries for each of the individual bats separately, related to Figure 3

(A–E) Population summaries for each of the 7 bats that were analyzed in main Figures 1, 2, and 3. These 7 bats were ordered here from the bat with the largest number of detected replay events (top row) to the lowest number (bottom row). On the left, we indicated the bat number, the tunnel length in which the bat was tested, the number of recording sessions, and the total number of replay events for that bat. (A–D) Distributions (probability density) of replay duration (A), compression ratio for replay speed (B), replay distance (C), and replay distance as a fraction of the tunnel length (D). Plotted similarly to main Figures 3A–3D. (E) Distributions (probability density) of replay positions along the tunnel. Each replay contributed to all the position bins that it covered. Individual lines indicate recording sessions, plotted separately for the two directions (two colors) for sleep (solid lines) and awake (dashed lines).

(F–J) Population summary for the bat from the 2-bat experiment, which was analyzed in main Figures 5C–5G. Shown are the same plots as in (A)–(E), plotted here for the bat recorded in the 2-bat experiment (the histograms in F–I show pooled data for sleep replays and awake replays).

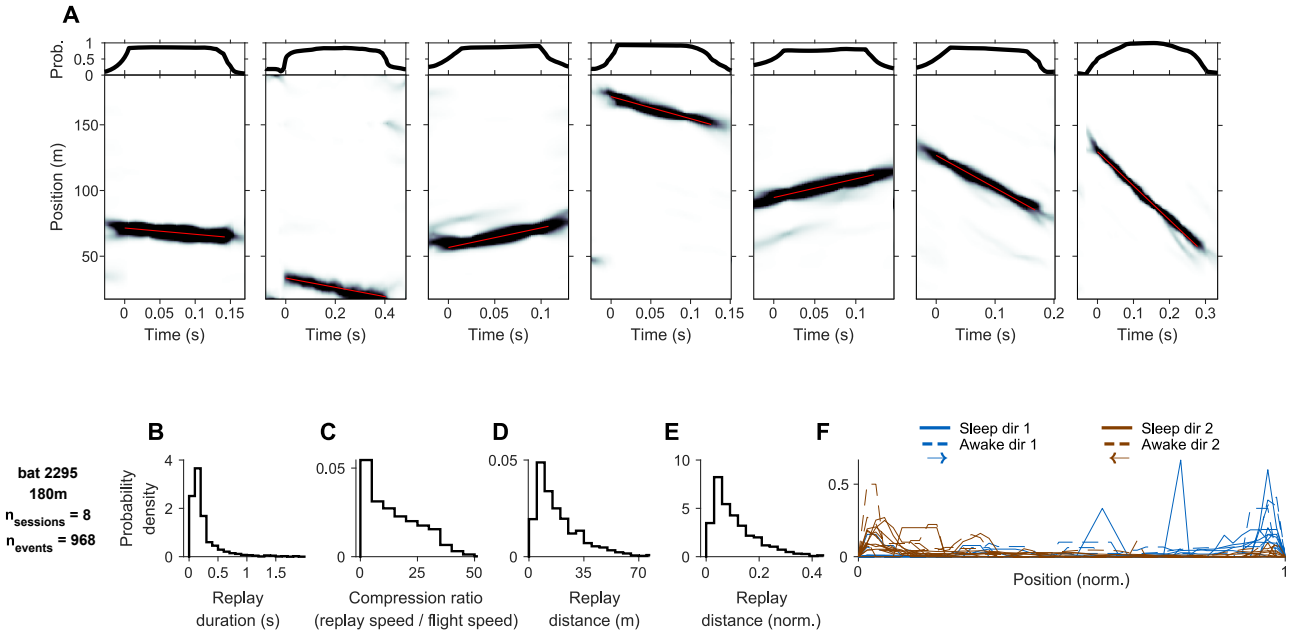

Figure S5. Example replays and population histograms for an additional bat, which was recorded in the long tunnel during a more complex experiment, related to Figure 3

This bat flew in a long 180-m tunnel, and alternated between a first session in which it performed choices in a T-junction at the end of the tunnel, and a second session in which it shuttled back-and-forth in the 180-m linear tunnel, without any choices. The data shown here are from the second session (back-and-forth shuttling in the linear tunnel, with no choices, similar to the 7 bats in the main experiment)—but because this bat performed overall a more complex task, we might expect somewhat longer replays—which indeed we found here.

(A) Examples of replays in this bat: many replays exhibited short replay distances (similar to replays in the 7 bats in Figures 1, 2, and 3 and to the bat from the 2-bat experiment), while some replays exhibited longer replay distances.

(B–E) Distributions (probability density) of replay duration (B), compression ratio for replay speed (C), replay distance (D), and replay distance as a fraction of the tunnel length (E). Pooled data for awake and sleep replays.

(F) Distributions (probability density) of replay positions along the tunnel, plotted as in Figure S4E.

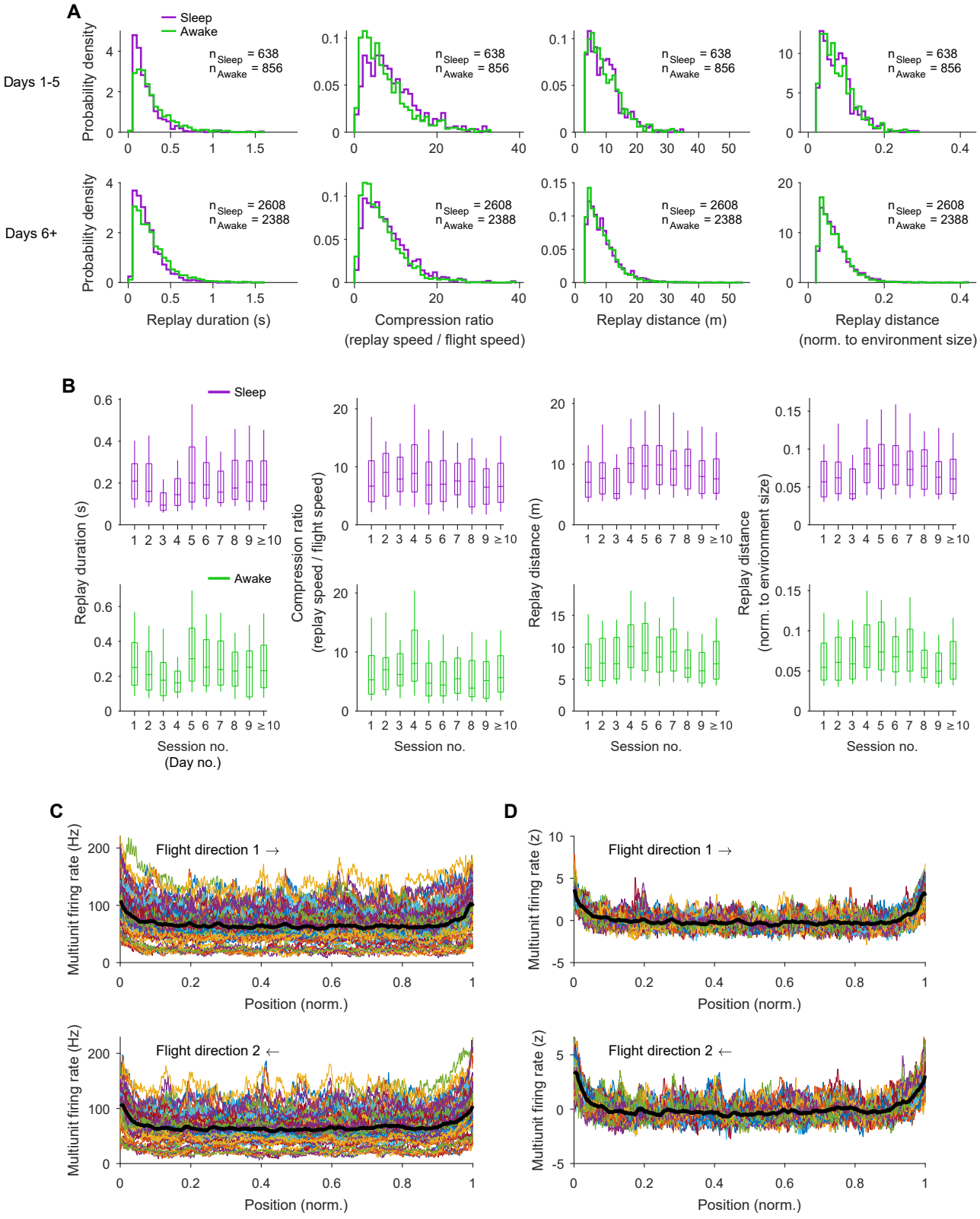

(legend on next page)

Figure S6. Replay was fragmented already on the first days in a novel environment, and multiunit firing rates were uniform along the tunnel for all the sessions, related to Figure 3

(A and B) Replay was fragmented already on the first days in a novel environment. Data from the two bats recorded in the 130-m tunnel: these bats were tested from the very first day of the bat's exposure to the tunnel (day 1). (A) Histograms of the replay duration, compression ratio for replay speed, replay distance, and replay distance normalized to environment size (columns)—plotted for the first 5 days in the long tunnel (top row), and for all the subsequent days (bottom row), separately for sleep replays (purple) and awake replays (green). Data pooled over both bats that were recorded from day 1. (B) Boxplots of replay parameters in individual days (sessions), from day 1 onward ("≥10": data pooled from day 10 and all the later days), for sleep replays (top) and awake replays (bottom). The boxplots show the median (horizontal line), 25%–75% percentiles (boxes) and 1%–99% percentiles (whiskers). Note the rather stable properties of replays already from day 1 (session 1).

(C and D) Multiunit firing rates were uniform along the tunnel for all the sessions (with increased rates at the tunnel ends). (C) Multiunit firing rates as a function of position, for individual sessions (colored lines, n = 82 sessions) and grand average (black line), plotted separately for the two flight directions (top and bottom; arrows show the flight direction). Note that for each individual session, the multiunit firing rates were relatively uniform along the tunnel (with increased firing rates at the tunnel ends). (D) Same as (C), with Z scored firing rates; the z-scoring was done separately for each session and each flight direction.

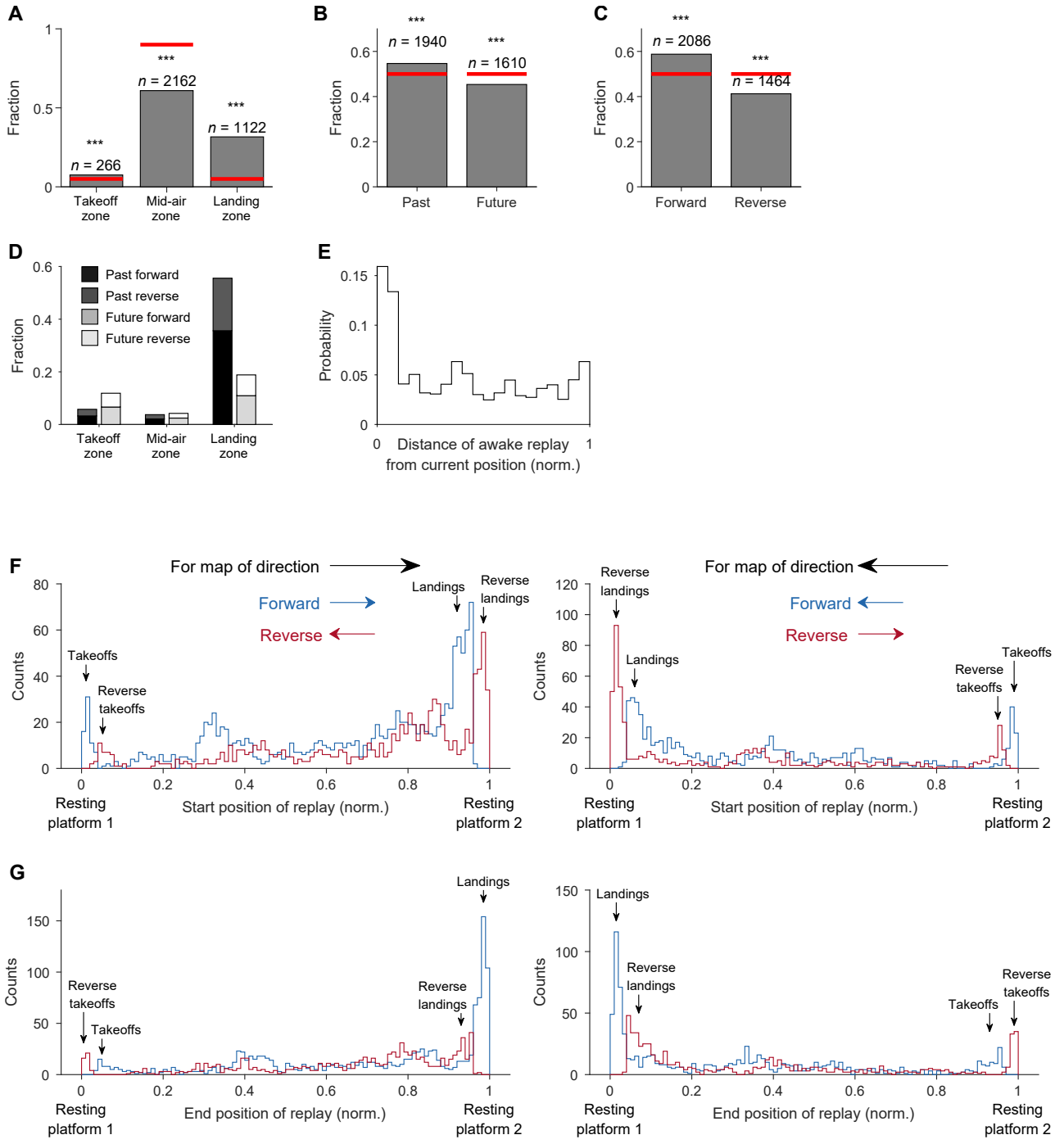

Figure S7. Fraction of awake replays that depicted different locations in the tunnel, past versus future, and forward versus reverse replays, related to Figure 3

Plotted only for awake replays (n = 3,550 replays from 82 sessions in 7 bats).

(A) Fraction of replays that represented the takeoff zone (the first 5% portion of the tunnel in each map direction), mid-air zone (the 90% central portion of the tunnel), and landing zone (the last 5% portion of the tunnel in each map direction). Numbers of replays are indicated. Red lines, chance levels (note that by chance, we would expect the fraction of replays in mid-air to be 18 times higher than in the takeoff or landing zones [90% / 5% = 18]). Stars, two-sided binomial test, compared with chance; ***$p < 0.001$ ($p = 5 \times 10^{-10}$ for takeoff, $p = 2 \times 10^{-308}$ for mid-air, and $p = 2 \times 10^{-79}$ for landing zone).

(B) Fraction of past replays and future replays (numbers of replays are indicated). Red lines, 50% chance level. Stars, two-sided binomial test, compared with chance; ***$p < 0.001$ ($p = 7 \times 10^{-8}$ for both past and future).

(legend continued on next page)

(C) Fraction of forward replays and reverse replays (numbers of replays are indicated). Red lines, 50% chance level. Stars, two-sided binomial test, compared with chance; ***$p < 0.001$ ($p = 10^{-25}$ for both forward and reverse).
(D) Fraction of replays that represented past and future, and forward and reverse replays—plotted separately for different locations of replays in the tunnel: takeoff zone, mid-air zone, and landing zone. Plotted similarly to Figure 3K but here sub-divided also to forward and reverse replays.
(E) Histogram of distances of awake replays from the current position of the bat, pooled for both resting platforms. Distance 0, close to the current platform (current position); distance 1, close to the far platform. Note that there were more local replays (close to the bat's current position) than remote replays (close to the far platform, namely far away from the bat's current position).
(F and G) Histograms of start positions (F) and end positions (G) of awake replays, plotted separately for each flight direction map (left and right; map direction indicated by black horizontal arrows above F). Blue, forward replay; red, reverse replay. Positions are normalized to the environment size; 0 and 1 are the two resting platforms at the two ends of the long tunnel.

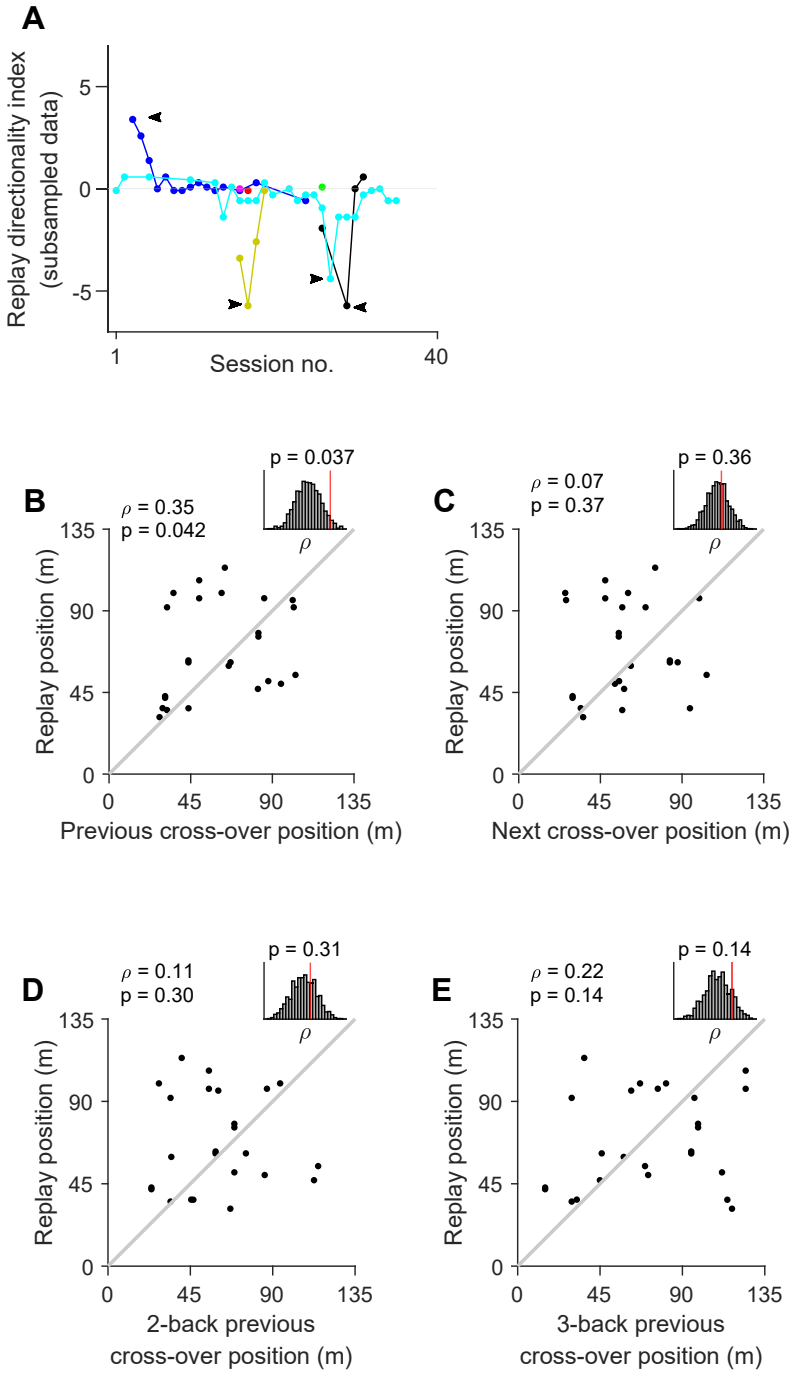

Figure S8. Behavioral relevance of replays: Additional controls, related to Figure 5

(A) Replay directionality index versus session no., plotted similarly to main Figure 5B—but here, instead of computing the index for the entire data in each session, we randomly subsampled 20 replays from the session and computed the directionality index for these 20 replays; this random subsampling was repeated 1,000 times for each session, and we plotted here for each session the median replay directionality index for the 1,000 subsamples for that session.

(B and C) Controls for the 2-bat experiment: similar plots to main Figures 5F and 5G but with different inclusion criteria. Data included in these two panels met an extra criterion that the replay had to belong to the same map direction as the direction of movement during the last cross-over. Dots depict the replay position versus the previous cross-over position (B) or versus the next cross-over position (C). Spearman correlations ρ are indicated. Insets plotted as in Figures 5F and 5G.

(D and E) Similar plots to main Figure 5F but plotting here the positions of the replays (dots) versus the positions of the 2-back previous cross-overs (D) or versus the positions of the 3-back previous cross-overs (E)—as opposed to the 1-back previous cross-overs plotted in main Figure 5F. Note that replay position exhibited significant correlations with the 1-back cross-over position (main Figure 5F) but *not* with the 2-back and 3-back cross-overs (D and E here).